JHEP

Published for SISSA by Springer

Received: May 28, 2014
Accepted: July 16, 2014
Published: August 7, 2014

JHEP08(2014)039

Z-Z' mixing and Z-mediated FCNCs in $\mathrm{SU}(3)_C \times \mathrm{SU}(3)_L \times \mathrm{U}(1)_X$ models

Andrzej J. Buras,[a,b] **Fulvia De Fazio**[c] **and Jennifer Girrbach-Noe**[a,b]

[a] *TUM Institute for Advanced Study, Lichtenbergstr. 2a, D-85748 Garching, Germany*

[b] *Physik Department, Technische Universität München, James-Franck-Straße, D-85748 Garching, Germany*

[c] *Istituto Nazionale di Fisica Nucleare, Sezione di Bari, Via Orabona 4, I-70126 Bari, Italy*

E-mail: andrzej.buras@tum.de, fulvia.defazio@ba.infn.it, jennifer.girrbach@tum.de

doi:10.1007/JHEP08(2014)039

Abstract: Most of the existing analyses of flavour changing neutral current processes (FCNC) in the 331 models, based on the gauge group $\mathrm{SU}(3)_C \times \mathrm{SU}(3)_L \times \mathrm{U}(1)_X$, are fully dominated by tree-level exchanges of a new heavy neutral gauge boson Z'. However, due to the $Z - Z'$ mixing also corresponding contributions from Z boson are present. As the $Z - Z'$ mixing is estimated generally in Z' models to be at most $\mathcal{O}(10^{-3})$, the latter contributions are usually neglected. The paucity of relevant parameters in 331 models allows to check whether this neglect is really justified in these concrete models. We calculate the impact of these contributions on $\Delta F = 2$ processes and rare K, B_s and B_d decays for different values of a parameter β, which distinguishes between various 331 models and for different fermion representations under the $\mathrm{SU}(3)_L$ group. We find a general expression for the $Z - Z'$ mixing in terms β, M_Z, $M_{Z'}$ and $\tan\bar{\beta}$, familiar from 2 Higgs Doublet models, that differs from the one quoted in the literature. We study in particular the models with $\beta = \pm n/\sqrt{3}$ with $n = 1, 2$ which have recently been investigated by us in the context of new data on $B_{s,d} \to \mu^+\mu^-$ and $B_d \to K^*(K)\mu^+\mu^-$. We find that these new contributions can indeed be neglected in the case of $\Delta F = 2$ transitions and decays, like $B_d \to K^*\mu^+\mu^-$, where they are suppressed by the small vectorial Z coupling to charged leptons. However, the contributions of tree-level Z exchanges to decays sensitive to axial-vector couplings, like $B_{s,d} \to \mu^+\mu^-$ and $B_d \to K\mu^+\mu^-$, and those with neutrinos in the final state, like $b \to s\nu\bar{\nu}$ transitions, $K^+ \to \pi^+\nu\bar{\nu}$ and $K_L \to \pi^0\nu\bar{\nu}$ cannot be generally neglected with size of Z contributions depending on β, $\tan\bar{\beta}$ and $M_{Z'}$. We analyze how our recent results on FCNCs in 331 models, in particular correlations between various observables, are modified by these new contributions. As a byproduct we analyze for the first time the ratio ε'/ε in these models including both Z' and Z contributions. Our analysis of electroweak precision observables within 331 models demonstrates transparently that the interplay of NP effects in electroweak precision observables and those in flavour observables could allow in the future to identify the favourite 331 model.

Keywords: Beyond Standard Model, Rare Decays, B-Physics, CP violation

ArXiv ePrint: 1405.3850

JHEP08(2014)039

Contents

JHEP08(2014)039

1 Introduction

An interesting class of dynamical models are the 331 models based on the gauge group $\mathrm{SU}(3)_C \times \mathrm{SU}(3)_L \times \mathrm{U}(1)_X$ [1, 2]. Detailed analyses of FCNC processes in these models have been presented by us in [3, 4]. Selection of earlier analyses of various aspects of these models related to flavour physics can be found in [5–15]. For other variants of 331 models see [16–18]. We briefly recall here only a few aspects of these models relevant for the analysis in this paper. As will be discussed in section 2.2, fermion representations under $\mathrm{SU}(3)_L$ transformations can be chosen in several ways. However, requirement of anomaly cancelation

and asymptotic freedom of QCD imposes that, for example, if two quark generations transform as triplets, the remaining one should be an antitriplet. An interesting relation connects the electric charge Q to the generators T_3, T_8 of SU(3) and the generator X of $\mathrm{U}(1)_X$: $Q = T_3 + \beta T_8 + X$, introducing the parameter β that plays a key role in this class of models.

Having an enlarged gauge group with respect to the SM, a number of new gauge bosons is present, whose charges depend on the value of β. However, independently of it, a new neutral gauge boson Z' is always present and can mediate FCNC at tree level in the quark sector. The Higgs sector is also enlarged. In particular, three Higgs triplets are present. Among these, two give masses to up and down type quarks, and the relative size of their vacuum expectation values will be important for our subsequent discussion. We shall introduce them later in section 2. Finally, also new heavy fermions are predicted to exist, but they do not play any role in our study and we shall not consider them any longer.

The nice feature of these models is a small number of free parameters which is lower than present in general Z' scenarios with left-handed flavour violating couplings to quarks considered in [19, 20]. This allows to find certain correlations between different meson systems which is not possible in the general case. Indeed the strength of the relevant Z' couplings to down-quarks is governed in these models by two mixing parameters, two CP-violating phases and the parameter β which defines a given 331 model up to the choice of fermion representations [8, 14] and determines the charges of new heavy fermions and gauge bosons as we have already mentioned above.

Thus for a given $M_{Z'}$ and β there are only four free parameters to our disposal. In particular for a given β, the diagonal couplings of Z' to quarks and leptons are fixed. Knowing these couplings simplifies the analysis significantly, increasing simultaneously the predictive power of the theory.

In [3] the relevant couplings have been presented for arbitrary β and in [4] a particular set of models with

$$\beta = \pm\frac{n}{\sqrt{3}}, \qquad n = 1, 2, 3 \tag{1.1}$$

has been analyzed. We have demonstrated that

- The models with $\beta = -2/\sqrt{3}$ and $\beta = -1/\sqrt{3}$ help in understanding the anomalies in $B_d \to K^*\mu^+\mu^-$ [21, 22] because in these models the coupling $\Delta_V^{\mu\bar{\mu}}(Z')$ is large.

- The models with $\beta = 2/\sqrt{3}$ and $\beta = 1/\sqrt{3}$ having significant $\Delta_A^{\mu\bar{\mu}}(Z')$ coupling provide interesting NP effects in $B_s \to \mu^+\mu^-$ that allow to bring the theory closer to the data [23–25].

- The model with $\beta = -\sqrt{3}$, advocated in particular in [26] in the context of $B_d \to K^*\mu^+\mu^-$ anomalies, has several problems originating in the presence of a Landau singularity for $\sin^2\theta_W = 0.25$. The same problem is found in the case $\beta = \sqrt{3}$. Therefore we will not consider them here.

We would like to emphasize here that these results have been obtained by assigning the fermions to specific fermion representations under $\mathrm{SU}(3)_L$ and that even for a given β the results listed above can change if the choice of representations is different. While it is known

JHEP08(2014)039

that the phenomenology of 331 models depends on the choice of fermion representations [8, 14] we recall some aspects of it below as this freedom has interesting consequences in the context of our analysis. Moreover, it clarifies certain differences between the analyses in [8, 14] and [3, 4].[1]

However, our previous analyses and to our knowledge all analyses of FCNC processes in 331 models neglected contributions from tree-level Z boson exchanges. Such contributions can be generated in 331 models by the $Z - Z'$ mixing but were expected to be very small as according to general analyses [27, 28] this mixing should be at most of $\mathcal{O}(10^{-3})$. In the absence of this mixing the Z couplings remain for a given electric quark charge flavour universal and in contrast to Z' gauge boson, there are no FCNCs mediated by Z boson at tree-level.

The goal of the present paper is to investigate, whether the neglect of Z boson FCNCs generated by $Z - Z'$ mixing in the 331 models in question is really justified. It will turn out that this is not always the case and we will investigate what is the impact of these new contributions on our results in [4]. Fortunately it will turn out that the determination of the allowed ranges for the parameters of the 331 models through $\Delta F = 2$ processes is unaffected by these new contributions. The same applies to our analysis of the anomalies in $B_d \to K^* \mu^+ \mu^-$. On the other hand in other decays considered by us Z contributions can be as large as Z' contributions so that for certain parameters and models the two contributions can cancel each other.

At this point we would like to emphasize that even if 331 models would not survive future flavour precision tests, they offer a very powerful laboratory to study not only correlations between various flavour observables but also between flavour observables and electroweak precision observables. One of the goals of our paper is to exhibit these correlations transparently.

Our paper is organized as follows. In section 2 we summarize some aspects of 331 models and present the general expression for the $Z - Z'$ mixing that differs from the one quoted in the literature [8, 14]. We also analyze for which processes and for which values of β the resulting FCNCs mediated by Z boson are relevant. We will frequently refer to our previous papers [3, 4], where all the details on the models considered can be found. In particular in the appendix A in [4] a compendium of all Z' couplings and Z couplings including their numerical values can be found. We will not repeat this compendium here but we will use it extensively in order to find out already in this section where the neglect of flavour violating Z exchanges is justified and where they have to be taken into account. In section 3 we show how our results in [3, 4] are modified through the inclusion of Z contributions. In section 4 we present for the first time the analysis of ε'/ε in 331 models and its correlation with rare K decays. In section 5 we reconsider the effects of $Z - Z'$ mixing in electroweak precision observables and discuss correlations between flavour and electroweak precision observables in 331 models in question. We conclude in section 6.

[1] We thank R. Martinez and F. Ochoa for discussions on this point.

JHEP08(2014)039

2 $Z - Z'$ mixing in 331 models

2.1 Basic formulae for $Z - Z'$ mixing

Among the new heavy particles in 331 models the most important role in flavour physics is played by a new Z' boson originating in the additional $\mathrm{U}(1)_X$ factor in the extended gauge group. The electroweak symmetry breaking is discussed in several papers quoted above and we will not repeat it here. It suffices to state that after the mass eigenstates for the SM fields, the photon and the Z boson have been constructed through appropriate rotation, there remains still small mixing between Z and Z' so that the heavy mass eigenstates are really

$$Z^1_\mu = \cos\xi Z_\mu + \sin\xi Z'_\mu, \qquad Z^2_\mu = -\sin\xi Z_\mu + \cos\xi Z'_\mu\,. \tag{2.1}$$

As $\sin\xi$ is estimated to be at most $\mathcal{O}(10^{-3})$ this mixing is usually neglected in FCNC processes so that the two mass eigenstates are simply $Z^1_\mu = Z_\mu$ and $Z^2_\mu = Z'_\mu$. Consequently only Z'_μ has flavour violating couplings in the mass eigenstate basis for quarks as a result of different transformation properties of the third generation under the extended gauge group. The flavour violating couplings of Z' are parametrized by complex couplings $\Delta^{ij}_L(Z')$ with $i, j = d, s, b$ in the present paper.

When the small but non-vanishing mixing represented by $\sin\xi$ is taken into account, not only the flavour violating couplings of the mass eigenstate Z^1_μ to quarks are generated but also its flavour diagonal couplings to SM fermions differ from the ones of the SM Z boson. Explicitly we have for $i \neq j$

$$\Delta^{ij}_L(Z^1) = \sin\xi\,\Delta^{ij}_L(Z') \equiv \Delta^{ij}_L(Z), \qquad \Delta^{ij}_L(Z^2) = \cos\xi\,\Delta^{ij}_L(Z') \approx \Delta^{ij}_L(Z'), \tag{2.2}$$

where in order not to modify the notation in flavour violating observables relative to our previous papers we will still use Z for Z^1 and Z' for Z^2 with masses M_Z and $M_{Z'}$, respectively. The small shifts in the masses of these gauge bosons relative to the case $\sin\xi = 0$ are irrelevant in flavour violating processes.

For flavour diagonal couplings to fermions (generically denoted with f) we have with $k = L, R, A, V$

$$\Delta^{ff}_k(Z^1) = \cos\xi\,\Delta^{ff}_k(Z) + \sin\xi\,\Delta^{ff}_k(Z'), \tag{2.3}$$

$$\Delta^{ff}_k(Z^2) = \cos\xi\,\Delta^{ff}_k(Z') - \sin\xi\,\Delta^{ff}_k(Z)\,. \tag{2.4}$$

In the calculations of flavour violating effects we can neglect the mixing effects in these couplings so that we can simply set

$$\Delta^{ff}_k(Z^1) = \Delta^{ff}_k(Z), \qquad \Delta^{ff}_k(Z^2) = \Delta^{ff}_k(Z') \tag{2.5}$$

as in our previous papers, but in the discussion of electroweak precision tests in section 5 we have to keep mixing effects in (2.3). Following [29] in this case we will use for the modified diagonal Z couplings to fermions

$$[\Delta^f_k(Z)]_{\rm eff} \equiv \cos\xi\,\Delta^{ff}_k(Z) + \sin\xi\,\Delta^{ff}_k(Z'). \tag{2.6}$$

JHEP08(2014)039

The second term in this equation allows then as we will see in the course of our analysis to select by means of electroweak precision observables the favourite 331 models.

Now the flavour violating Z' couplings to quarks, for the three meson systems K, B_d and B_s,

$$\Delta_L^{sd}(Z'), \qquad \Delta_L^{bd}(Z'), \qquad \Delta_L^{bs}(Z') \tag{2.7}$$

depend on the elements v_{ij} of a mixing matrix V_L. Being proportional to $v_{32}^* v_{31}$, $v_{33}^* v_{31}$ and $v_{33}^* v_{32}$, respectively, they depend only on four new parameters (explicit formulae are given in [3]):

$$\tilde{s}_{13}, \quad \tilde{s}_{23}, \quad \delta_1, \quad \delta_2\,. \tag{2.8}$$

Here $\tilde{s}_{13}$ and $\tilde{s}_{23}$ are positive definite and δ_i in the range $[0, 2\pi]$. Therefore for fixed $M_{Z'}$ and β, the Z' contributions to all processes analyzed by us depend only on these parameters implying very strong correlations between NP contributions to various observables. Indeed, the B_d system involves only the parameters $\tilde{s}_{13}$ and δ_1 while the B_s system depends on $\tilde{s}_{23}$ and δ_2. Moreover, stringent correlations between observables in $B_{d,s}$ sectors and in the kaon sector are found since kaon physics depends on $\tilde{s}_{13}$, $\tilde{s}_{23}$ and $\delta_2 - \delta_1$. A very constraining feature of this models is that the diagonal couplings of Z' to quarks and leptons are fixed for a given β, except for a weak dependence on $M_{Z'}$ due to running of $\sin^2\theta_W$.

As the mass M_Z and flavour diagonal Z-couplings to all SM fermions are known, the model is also predictive after the inclusion of $Z - Z'$ mixing, although one additional parameter, $\tan\bar{\beta}$, enters the game. This mixing has been calculated in [8] in terms of the $\mathrm{SU}(3)_L$ and $\mathrm{U}(1)_X$ gauge couplings and the relevant vacuum expectations values but for our purposes it is useful to express it in terms of measurable quantities and β. Repeating this calculation we find an important expression

$$\sin\xi = \frac{c_W^2}{3}\sqrt{f(\beta)}\left(3\beta\frac{s_W^2}{c_W^2} + \sqrt{3}a\right)\left[\frac{M_Z^2}{M_{Z'}^2}\right] \equiv B(\beta, a)\left[\frac{M_Z^2}{M_{Z'}^2}\right], \tag{2.9}$$

where

$$f(\beta) = \frac{1}{1 - (1+\beta^2)s_W^2} > 0, \tag{2.10}$$

$s_W^2 = \sin^2\theta_W$ and

$$-1 < a = \frac{v_-^2}{v_+^2} < 1 \tag{2.11}$$

with $v_\pm^2$ given in terms of the vacuum expectation values of two Higgs triplets ρ and η as follows

$$v_+^2 = v_\eta^2 + v_\rho^2, \qquad v_-^2 = v_\eta^2 - v_\rho^2\,. \tag{2.12}$$

As the Higgs system responsible for the breakdown of the SM group has the structure of a two Higgs doublet model and the triplets ρ and η are responsible for the masses of up-quarks and down-quarks respectively one can express the parameter a in terms of the usual $\tan\bar{\beta}$ where we introduced a *bar* to distinguish the usual angle β from the parameter β in 331 models. We have then

$$a = \frac{1 - \tan^2\bar{\beta}}{1 + \tan^2\bar{\beta}}, \qquad \tan\bar{\beta} = \frac{v_\rho}{v_\eta}. \tag{2.13}$$

JHEP08(2014)039

Thus for $\tan\bar{\beta} = 1$ the parameter $a = 0$ which simplifies the formula for $\sin\xi$ relating uniquely its sign to the sign of β. On the other hand in the large $\tan\bar{\beta}$ limit we find $a = -1$ and in the low $\tan\bar{\beta}$ limit one has $a = 1$.

We have emphasized in [4] that the couplings $\Delta_L^{ij}(Z')$ should be evaluated at $\mu = M_{Z'}$ and this implies that the s_W^2 entering these couplings should be evaluated at $\mu = M_{Z'}$. In evaluating $\Delta_L^{ij}(Z)$ by means of (2.2) such Z'-couplings should be used. However, as the $Z - Z'$ mixing is generated in the process of the SM electroweak symmetry breaking, in evaluating $\sin\xi$ by means of (2.9) and subsequently $\Delta_L^{ij}(Z)$ by means of (2.2) the value of s_W^2 at $\mu = M_Z$ should be used.

Our result for $\sin\xi$ differs from the one that one would obtain from the formula given in [8, 14] by expressing it in terms of s_W, c_W, M_Z and $M_{Z'}$. We find opposite overall sign and the factor $\sqrt{3}$ in front of the parameter a that is missing in [8, 14].[2] The difference in sign is important for the interference between NP contributions from Z and Z' exchanges and consequently for the pattern of NP effects. It is also crucial for the interplay of flavour physics with electroweak precision tests and should also have an impact on the analyses of $Z - Z'$ mixing effects in [8, 9, 14]. But these correlations depend also on the value of $\tan\bar{\beta}$ and we will see this explicitly below.

The expression in (2.9) tells us indeed that $\sin\xi$ is very small but one should remember that the propagator suppression of FCNC transitions in the case of Z' is by a factor of $M_{Z'}^2/M_Z^2$ stronger than in the case of Z at the amplitude level. Therefore we should make a closer look at the values of $\sin\xi$ and Z' couplings to leptons as functions of β and $\tan\bar{\beta}$ and compare them with the known Z couplings to fermions in order to decide whether Z boson contributions to FCNC processes can be neglected or not. However first we have to elaborate on the choice of fermion representations.

2.2 Choice of fermion representations

As already emphasized in [8, 14] the choice of β does not uniquely specify the phenomenology of the 331 model considered which further depends on the choice of fermion representations under $\mathrm{SU}(3)_L$. Here we discuss some aspects of this dependence that are relevant for our study.

Our choice of representations in [3, 4] under $\mathrm{SU}(3)_L$ can be summarized as follows. The first two generations of quarks are put into triplets (3) while the third one into the antitriplet (3^*):

$$\begin{pmatrix} u \\ d \\ D \end{pmatrix}_L \qquad \begin{pmatrix} c \\ s \\ S \end{pmatrix}_L \qquad \begin{pmatrix} b \\ -t \\ T \end{pmatrix}_L . \tag{2.14}$$

[2] The authors of these papers confirm our findings [30].

JHEP08(2014)039

The corresponding right handed quarks are singlets. The anomaly cancellation then requires that leptons are put into antitriplets:

$$\begin{pmatrix} e \\ -\nu_e \\ E_e \end{pmatrix}_L \qquad \begin{pmatrix} \mu \\ -\nu_\mu \\ E_\mu \end{pmatrix}_L \qquad \begin{pmatrix} \tau \\ -\nu_\tau \\ E_\tau \end{pmatrix}_L . \tag{2.15}$$

We refer to this choice as F_1.

On the other hand in [8, 14] the triplets and antitriplets are interchanged relative to our choice. That is the first two quark generations are in antitriplets while the third one in a triplet. Therefore leptons are also in triplets. We call this fermion assignment F_2.[3]

The important two features to be remembered for our discussion below is that for a given β:

- The expression for $\sin\xi$ in (2.9) is independent of whether F_1 or F_2 is used.
- On the other hand as evident from the comparison of our compendium for Z' couplings to fermions in [4] with table 4 of [14] the signs in front of β in these couplings are changed when going from F_1 to F_2. This property can be derived from the action of the relevant operator $\hat{Q}_W$ on triplet and antitriplet. See formulae in section 2 of [3].

These observations have the following important phenomenological implications given here first without FCNCs due to Z boson:

- In F_1 scenario the models with $\beta = -2/\sqrt{3}$ and $\beta = -1/\sqrt{3}$ are useful for the explanation of the anomalies in $B_d \to K^*\mu^+\mu^-$ because with F_1 representations the coupling $\Delta_V^{\mu\bar{\mu}}(Z')$ is large. On the other hand the models with $\beta = 2/\sqrt{3}$ and $\beta = 1/\sqrt{3}$ having significant $\Delta_A^{\mu\bar{\mu}}(Z')$ coupling provide interesting NP effects in $B_{s,d} \to \mu^+\mu^-$.
- In F_2 scenario the situation is reversed. The models with $\beta = 2/\sqrt{3}$ and $\beta = 1/\sqrt{3}$ are useful for the explanation of the anomalies in $B_d \to K^*\mu^+\mu^-$ while the ones with $\beta = -2/\sqrt{3}$ and $\beta = -1/\sqrt{3}$ for $B_{s,d} \to \mu^+\mu^-$.
- While these two scenarios cannot be distinguished by flavour observables when only Z' contributions are considered they can be distinguished when Z boson contributions are taken into account. This originates in the fact that the $\sin\xi$ entering the $\Delta_L^{ij}(Z)$ couplings in (2.2) *does depend* on the sign of β but *does not depend* on whether F_1 scenario or F_2 scenario is considered. In other words the invariance in flavour observables under the transformations

$$\beta \to -\beta, \qquad F_1 \to F_2 \tag{2.16}$$

present in the absence of $Z - Z'$ mixing is broken by this mixing. We will see this explicitly in our numerical analysis below.

[3] In [8, 14] still two other quark assignments are discussed in which the first or the second quark generation transforms differently under $\mathrm{SU}(3)_L$ than the remaining two. But we find the ones listed above more natural due to large top quark mass and we do not discuss these two additional possibilities.

JHEP08(2014)039

- As a particular sign of β could be favoured by flavour conserving observables, in particular electroweak precision tests, this feature allows in principle to determine whether the representation F_1 or F_2 is favoured by nature. We will see this explicitly in section 5.

2.3 $\Delta F = 2$ processes

In the models considered only SM $\Delta F = 2$ operator (i.e. that changes flavour quantum number by two units, as for example in neutral meson mixing) in each meson system is present and the effects of NP in all $\Delta F = 2$ transitions can be compactly summarized by generally flavour dependent shifts ΔS in the SM one loop function S that is flavour independent. However due to the relation (2.2) the flavour dependence of the shifts ΔS due to Z and Z' contributions is the same. Consequently for all meson systems the ratio of the shifts in S due to Z and Z' is given universally as follows:

$$\frac{\Delta S(Z)}{\Delta S(Z')} = \sin^2\xi \left[\frac{M_{Z\prime}^2}{M_Z^2}\right] = B^2(\beta,a)\left[\frac{M_Z^2}{M_{Z'}^2}\right]. \tag{2.17}$$

As $B(\beta,a) \le 1.1$ in all four models considered by us, it follows that Z contributions to all $\Delta F = 2$ transitions can be neglected. This is good news: the determination of the allowed values of the new parameters (2.8) by means of $\Delta F = 2$ processes remains unmodified relative to our analyses in [3, 4].

2.4 $\Delta F = 1$ processes

It should be noted that in $\Delta F = 2$ processes the flavour violating coupling of Z enters twice which resulted in $\sin^2\xi$ dependence in the $\Delta F = 2$ amplitudes. However, in $\Delta F = 1$ amplitudes (implying a change by one unit of flavour quantum number, as in weak decays) it appears only once, whereas the dependence on the mass of the exchanged gauge boson remains unchanged. Again the flavour dependence in the vertex involving quarks is the same for Z and Z' and as the operators in each systems are also the same, the ratio of the amplitudes $A_{\ell\ell}(Z)$ and $A_{\ell\ell}(Z')$ takes a very simple form:

$$R_{\ell\ell}^k = \frac{A_{\ell\ell}(Z)}{A_{\ell\ell}(Z')} = \sin\xi \left[\frac{M_{Z\prime}^2}{M_Z^2}\right]\left[\frac{\Delta_k^{\ell\ell}(Z)}{\Delta_k^{\ell\ell}(Z')}\right] = B(\beta,a)\left[\frac{\Delta_k^{\ell\ell}(Z)}{\Delta_k^{\ell\ell}(Z')}\right], \tag{2.18}$$

where $k = L, R, A, V$ and $\ell\ell$ stands either for charged leptons or neutrinos in the final state. The remarkable property of this formula is its independence on $M_{Z'}$. Consequently the ratios $R_{\ell\ell}^k$ with known Z couplings to leptons are only functions of β and of the parameter a or equivalently $\tan\bar\beta$. In addition they depend on whether the representation F_1 or F_2 is considered.

The ratios $R_{\ell\ell}^k$ give us the information on the importance of Z contributions relatively to Z' contributions but in order to get the full picture, in particular in view of the dependence of NP effects on the choice of fermion representations, it is useful to consider the quantities

$$W_{\ell\ell}^k = \Delta_k^{\ell\ell}(Z')\left(1 + R_{\ell\ell}^k\right), \tag{2.19}$$

which will directly enter the phenomenological expressions.

JHEP08(2014)039

β	$-\frac{2}{\sqrt{3}}$	$-\frac{1}{\sqrt{3}}$	$\frac{1}{\sqrt{3}}$	$\frac{2}{\sqrt{3}}$
$\sin\xi$ $[10^{-3}]$	$-0.36(-0.92)$	$-0.15(-0.60)$	$0.15(-0.31)$	$0.36(-0.19)$
$R_V^{\mu\mu}$	$0.015(0.038)$	$0.012(0.047)$	$-4.36(9.02)$	$0.046(0.024)$
$R_A^{\mu\mu}$	$1.77(4.50)$	$0.46(1.88)$	$-0.23(0.48)$	$-0.36(0.19)$
$R_L^{\nu\nu}$	$-0.36(-0.91)$	$-0.23(-0.94)$	$0.46(-0.95)$	$1.77(-0.95)$
$W_V^{\mu\mu}$	$0.74(0.76)$	$0.39(0.41)$	$-0.0035(0.010)$	$-0.25(-0.24)$
$\Delta_V^{\mu\mu}(Z')$	0.731	0.386	0.001	-0.242
$W_A^{\mu\mu}$	$-0.23(-0.45)$	$-0.19(-0.37)$	$-0.20(-0.38)$	$-0.26(-0.49)$
$\Delta_A^{\mu\mu}(Z')$	-0.082	-0.130	-0.258	-0.407
$W_L^{\nu\nu}$	$0.26(0.036)$	$0.20(0.015)$	$0.19(0.0060)$	$0.23(0.0042)$
$\Delta_L^{\nu\nu}(Z')$	0.407	0.258	0.130	0.082
$R_{\varepsilon'}$	$-0.12(-0.31)$	$-0.12(-0.50)$	$-0.12(0.25)$	$-0.12(0.066)$

Table 1. $\sin\xi$, $R_{V,A,L}^{\mu\mu}$, $W_{V,A,L}^{\mu\mu}$, $\Delta_{V,A,L}^{\mu\mu,\nu\nu}$ and $R_{\varepsilon'}$ from (4.19) for different β and $\tan\bar{\beta} = 1(5)$ in scenario F_1 for fermion representations and for $M_{Z'} = 3\,\text{TeV}$. $R_{\varepsilon'}$ is defined in (4.18).

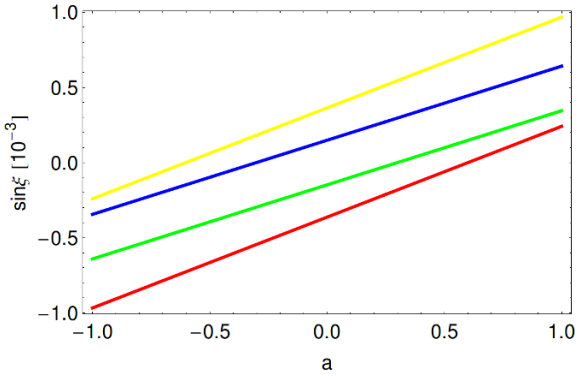

Figure 1. $\sin\xi$ as a function of a for different β ($-\frac{2}{\sqrt{3}}$: red, $-\frac{1}{\sqrt{3}}$: green, $\frac{1}{\sqrt{3}}$: blue, $\frac{2}{\sqrt{3}}$: yellow) and for $M_{Z'} = 3\,\text{TeV}$.

In table 1 we show the values of $\sin\xi$, $R_{\ell\ell}^k$ and $W_{\ell\ell}^k$ relevant for the couplings $\Delta_V^{\mu\mu}$, $\Delta_A^{\mu\mu}$ and $\Delta_L^{\nu\nu}$ in scenario F_1 for fermion representations for the four values of β and two values of $\tan\bar{\beta} = 1(5)$. The corresponding results for scenario F_2 are given in table 2 and for $\tan\bar{\beta} = 0.2$ and $F_1(F_2)$ in table 3. In these tables we fix $M_{Z'} = 3\,\text{TeV}$, as we do in our numerical analysis.

In figure 1 we show $\sin\xi$ as a function of a for different values of β. The values $a = 0$ and $a = -12/13(12/13)$ correspond to $\tan\bar{\beta} = 1$ and $\tan\bar{\beta} = 5(0.2)$, respectively.

We observe the following features:

- In the case of decays involving the coupling $\Delta_V^{\mu\mu}(Z)$ the contributions from Z boson can be neglected due its small vectorial coupling to charged leptons. The large values

JHEP08(2014)039

β	$-\frac{2}{\sqrt{3}}$	$-\frac{1}{\sqrt{3}}$	$\frac{1}{\sqrt{3}}$	$\frac{2}{\sqrt{3}}$
$\sin\xi$ $[10^{-3}]$	$-0.36(-0.92)$	$-0.15(-0.60)$	$0.15(-0.31)$	$0.36(-0.19)$
$R_V^{\mu\mu}$	$-0.046(-0.12)$	$4.36(17.7)$	$-0.012(0.024)$	$-0.015(0.0081)$
$R_A^{\mu\mu}$	$0.36(0.91)$	$0.23(0.94)$	$-0.46(0.95)$	$-1.77(0.95)$
$R_L^{\nu\nu}$	$-1.77(-4.50)$	$-0.46(-1.87)$	$0.23(-0.48)$	$0.36(-0.19)$
$W_V^{\mu\mu}$	$-0.23(-0.21)$	$0.0055(0.019)$	$0.38(0.40)$	$0.72(0.74)$
$\Delta_V^{\mu\mu}(Z')$	-0.242	0.001	0.386	0.731
$W_A^{\mu\mu}$	$-0.55(0.78)$	$-0.32(-0.50)$	$-0.070(-0.25)$	$0.064(-0.16)$
$\Delta_A^{\mu\mu}(Z')$	-0.407	-0.258	-0.130	-0.082
$W_L^{\nu\nu}$	$-0.064(-0.29)$	$0.070(-0.11)$	$0.32(0.13)$	$0.55(0.33)$
$\Delta_L^{\nu\nu}(Z')$	0.082	0.130	0.258	0.407
$R_{\varepsilon'}$	$0.12(0.31)$	$0.12(0.50)$	$0.12(-0.25)$	$0.12(-0.066)$

Table 2. $\sin\xi$, $R_{V,A,L}^{\mu\mu}$, $W_{V,A,L}^{\mu\mu}$, $\Delta_{V,A,L}^{\mu\mu,\nu\nu}$ and $R_{\varepsilon'}$ from (4.19) for different β and $\tan\bar{\beta} = 1(5)$ in scenario F_2 for fermion representations and for $M_{Z'} = 3\,\text{TeV}$. $R_{\varepsilon'}$ is defined in (4.18).

β	$-\frac{2}{\sqrt{3}}$	$-\frac{1}{\sqrt{3}}$	$\frac{1}{\sqrt{3}}$	$\frac{2}{\sqrt{3}}$
$\sin\xi$ $[10^{-3}]$	$0.194(0.194)$	$0.307(0.307)$	$0.603(0.603)$	$0.921(0.921)$
$R_V^{\mu\mu}$	$-0.008(0.024)$	$-0.024(-9.02)$	$-17.73(-0.047)$	$0.115(-0.038)$
$R_A^{\mu\mu}$	$-0.950(-0.192)$	$-0.954(-0.479)$	$-0.942(-1.876)$	$-0.912(-4.500)$
$R_L^{\nu\nu}$	$0.192(0.950)$	$0.479(0.954)$	$1.876(0.942)$	$4.500(0.912)$
$W_V^{\mu\mu}$	$0.725(-0.248)$	$0.377(-0.008)$	$-0.017(0.368)$	$-0.270(0.703)$
$W_A^{\mu\mu}$	$-0.004(-0.328)$	$-0.006(-0.134)$	$-0.015(0.113)$	$-0.036(0.288)$
$W_L^{\nu\nu}$	$0.485(0.160)$	$0.381(0.253)$	$0.372(0.501)$	$0.453(0.778)$
$R_{\varepsilon'}$	$0.066(-0.066)$	$0.25(-0.25)$	$-0.50(0.50)$	$-0.31(0.31)$

Table 3. $\sin\xi$, $R_{V,A,L}^{\mu\mu}$, $W_{V,A,L}^{\mu\mu}$ and $R_{\varepsilon'}$ from eq. (4.19) for different β and $\tan\bar{\beta} = 0.2$ in scenario F_1 (F_2) for fermion representations and for $M_{Z'} = 3\,\text{TeV}$. $R_{\varepsilon'}$ is defined in (4.18).

of $R_{\mu\mu}^V$ for $\beta = 1/\sqrt{3}$ in the case of F_1 and $\beta = -1/\sqrt{3}$ in the case of F_2 do not imply large contribution of Z boson as in this case Z' contribution is negligible. This is good news. The explanation of $B_d \to K^*\mu^+\mu^-$ anomalies with Z' contributions presented in [4] remains basically unmodified.

- But in the case of $B_{s,d} \to \mu^+\mu^-$, $B_d \to K\mu^+\mu^-$ and decays with neutrinos in the final state, like $b \to s\nu\bar{\nu}$ transitions, $K^+ \to \pi^+\nu\bar{\nu}$ and $K_L \to \pi^0\nu\bar{\nu}$ Z contributions cannot be generally neglected but the size of the additional contributions depends on β and $\tan\bar{\beta}$.

JHEP08(2014)039

- Comparing tables 1 and 2 we observe that indeed the symmetry (2.16) is broken by $Z - Z'$ mixing. This is also seen in table 3.
- Finally, we emphasize that the pattern of NP effects is governed by the sign of $\sin\xi$ in (2.9).

In the next section we will investigate these new contributions numerically.

3 Z contributions to $\Delta F = 1$ observables

3.1 Preliminaries

The inclusion of flavour violating effects from Z in the observables analyzed in [4] amounts to replacing the shifts due to NP in SM one-loop functions, given in the formulae (22)–(27) in that paper, by the following ones.

Defining

$$g_{\rm SM}^2 = 4\frac{G_F}{\sqrt{2}}\frac{\alpha}{2\pi\sin^2\theta_W}\,, \qquad \lambda_i^{(K)} = V_{is}^* V_{id}, \qquad \lambda_t^{(q)} = V_{tb}^* V_{tq} \tag{3.1}$$

one has for decays $B_q \to \mu^+\mu^-$ with $q = d, s$ governed by the function Y

$$\Delta Y(B_q) = \left[\frac{\Delta_A^{\mu\bar\mu}(Z')}{M_{Z'}^2 g_{\rm SM}^2}\right]\frac{\Delta_L^{qb}(Z')}{V_{tq}^* V_{tb}}(1 + R_{\mu\mu}^A) \tag{3.2}$$

and for $K_L \to \mu^+\mu^-$

$$\Delta Y(K) = \left[\frac{\Delta_A^{\mu\bar\mu}(Z')}{M_{Z'}^2 g_{\rm SM}^2}\right]\frac{\Delta_L^{sd}(Z')}{V_{ts}^* V_{td}}(1 + R_{\mu\mu}^A). \tag{3.3}$$

Similarly for $b \to q\nu\bar\nu$ transitions governed by the function X one finds

$$\Delta X(B_q) = \left[\frac{\Delta_L^{\nu\nu}(Z')}{g_{\rm SM}^2 M_{Z'}^2}\right]\frac{\Delta_L^{qb}(Z')}{V_{tq}^* V_{tb}}(1 + R_{\nu\nu}^L) \tag{3.4}$$

and for $K^+ \to \pi^+\nu\bar\nu$ and $K_L \to \pi^0\nu\bar\nu$

$$\Delta X(K) = \left[\frac{\Delta_L^{\nu\bar\nu}(Z')}{g_{\rm SM}^2 M_{Z'}^2}\right]\frac{\Delta_L^{sd}(Z')}{V_{ts}^* V_{td}}(1 + R_{\nu\nu}^L). \tag{3.5}$$

The corrections from NP to the Wilson coefficients C_9 and C_{10} that weight the semileptonic operators in the effective hamiltonian relevant for $b \to s\mu^+\mu^-$ transitions and used in the recent literature are given as follows

$$\sin^2\theta_W C_9^{\rm NP} = -\frac{1}{g_{\rm SM}^2 M_{Z'}^2}\frac{\Delta_L^{sb}(Z')\Delta_V^{\mu\bar\mu}(Z')}{V_{ts}^* V_{tb}}(1 + R_{\mu\mu}^V), \tag{3.6}$$

$$\sin^2\theta_W C_{10}^{\rm NP} = -\frac{1}{g_{\rm SM}^2 M_{Z'}^2}\frac{\Delta_L^{sb}(Z')\Delta_A^{\mu\bar\mu}(Z')}{V_{ts}^* V_{tb}}(1 + R_{\mu\mu}^A). \tag{3.7}$$

As seen in these equations $C_9^{\rm NP}$ involves leptonic vector coupling of Z' while $C_{10}^{\rm NP}$ the axial-vector one. $C_9^{\rm NP}$ is crucial for $B_d \to K^*\mu^+\mu^-$, $C_{10}^{\rm NP}$ for $B_s \to \mu^+\mu^-$ and both coefficients are relevant for $B_d \to K\mu^+\mu^-$.

JHEP08(2014)039

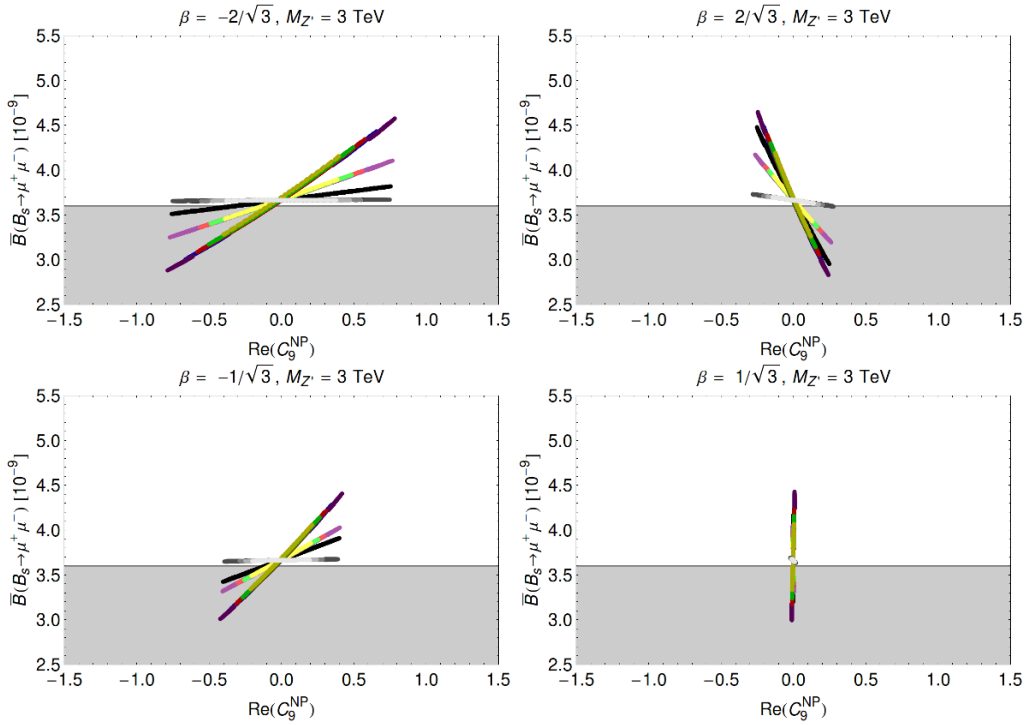

Figure 2. Correlation $\overline{\mathcal{B}}(B_s \to \mu^+\mu^-)$ versus $\mathrm{Re}(\mathrm{C}_9^{\mathrm{NP}})$ in models with F_1 for $\beta = \pm 1/\sqrt{3}$ and $\beta = \pm 2/\sqrt{3}$ setting $M_{Z'} = 3\,\mathrm{TeV}$ and different values of C_{B_s} ($C_{B_s} = 0.90 \pm 0.01, 0.96 \pm 0.01, 1.00 \pm 0.01$, $C_{B_s} = 1.04 \pm 0.01, 1.10 \pm 0.01$ (yellow, green, red, blue, purple; from light gray to dark gray)). Black is without $Z - Z'$-mixing, lighter colours are for $\tan\bar{\beta} = 1$, darker colours for $\tan\bar{\beta} = 5$ and gray colours for $\tan\bar{\beta} = 0.2$. The gray regions show the experimental range $\overline{\mathcal{B}}(B_s \to \mu^+\mu^-) = (2.9 \pm 0.7) \cdot 10^{-9}$.

3.2 Numerical results for B decays

Before presenting our results we recall the present SM value for $B_s \to \mu^+\mu^-$ [31]

$$\overline{\mathcal{B}}(B_s \to \mu^+\mu^-)_{\mathrm{SM}} = (3.65 \pm 0.23) \times 10^{-9}, \quad \overline{\mathcal{B}}(B_s \to \mu^+\mu^-)_{\mathrm{exp}} = (2.9 \pm 0.7) \times 10^{-9}, \tag{3.8}$$

where we have also shown the latest average of the results from LHCb and CMS [23–25]. The agreement of the SM prediction with the data for $B_s \to \mu^+\mu^-$ in (3.8) is remarkable, although the rather large experimental error still allows for sizable NP contributions with the ones suppressing the branching ratio relative to its SM value being favoured.

As far as the anomalies in $B_d \to K^*\mu^+\mu^-$ [21, 22] are concerned a number of analyses, of which we only quote three [32–34], indicate that $\mathrm{Re}(\mathrm{C}_9^{\mathrm{NP}}) = -1.0 \pm 0.5$. Thus in the plots presented below the results with

$$\overline{\mathcal{B}}(B_s \to \mu^+\mu^-) < \overline{\mathcal{B}}(B_s \to \mu^+\mu^-)_{\mathrm{SM}}, \qquad \mathrm{Re}(\mathrm{C}_9^{\mathrm{NP}}) \leq -0.5 \tag{3.9}$$

are favoured by the present data.

The results for various observables in 331 models with fermion representations F_1 have been presented in figures 5–17 in [4]. The present analysis shows how the latter results are

JHEP08(2014)039

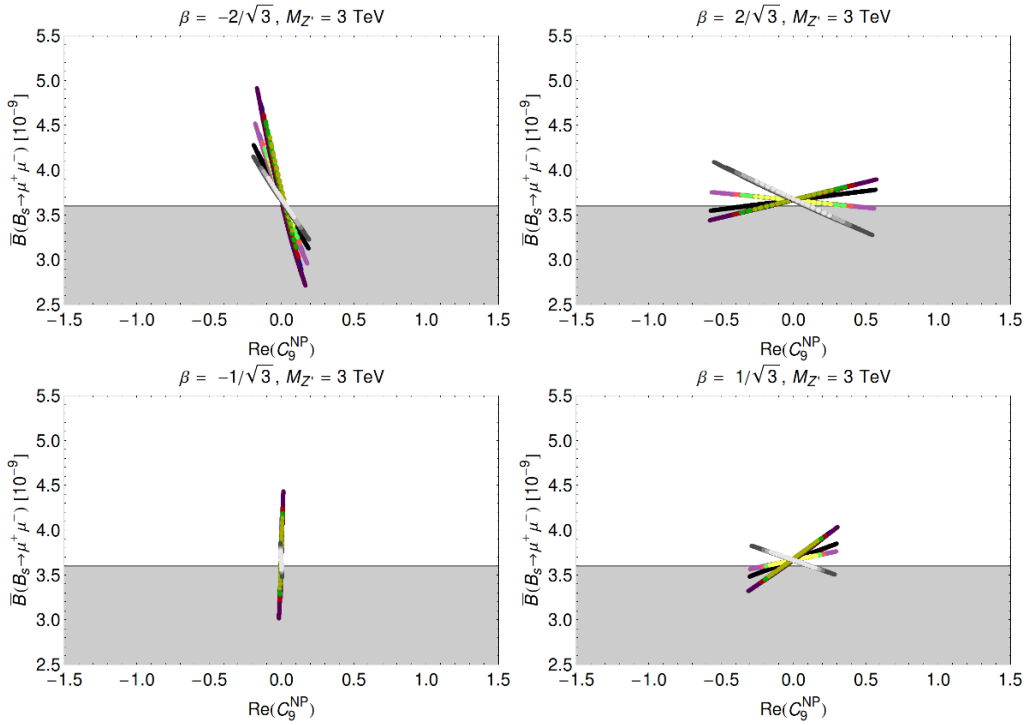

Figure 3. As in figure 2 but for F2.

modified when Z boson contributions are included and when the fermion representations F_2 are considered instead of F_1.

First of all taking into account that the Z contributions can be neglected in all $\Delta F = 2$ transitions and in the coefficient C_9 the results in figures 7 and 8 in [4] remain basically unchanged as they involve only $\Delta F = 2$ observables and C_9. On the other hand in the processes in which NP is governed by the shifts in (3.2)–(3.5) and C_{10} we find that modifications can be sizable, in particular when two observables taking part in the correlation are affected by Z contributions in a rather different manner.

In order to have appropriate comparison with the results in [4] we use the same treatment of CKM parameters and hadronic uncertainties as in the latter paper so that the difference between various correlations are only due to differences in NP contributions. For this reason we do not list the input parameters that can be found in table 3 of that paper.

The colour coding in the plots presented in this subsection is as follows:

- The results of [4] and those new ones in fermion representations F_2 that include only Z' contributions are presented in *black*.

- The results that include both Z' and Z contributions are given in colours that distinguish between the values of $C_{B_s} = \Delta M_s/(\Delta M_s)_{\rm SM}$.

- As for a given β the contributions from Z boson depend on $\tan\bar{\beta}$, we show the results for $\tan\bar{\beta} = 1$ in light colours, for $\tan\bar{\beta} = 5$ in darker colours and for $\tan\bar{\beta} = 0.2$ in gray colours.

JHEP08(2014)039

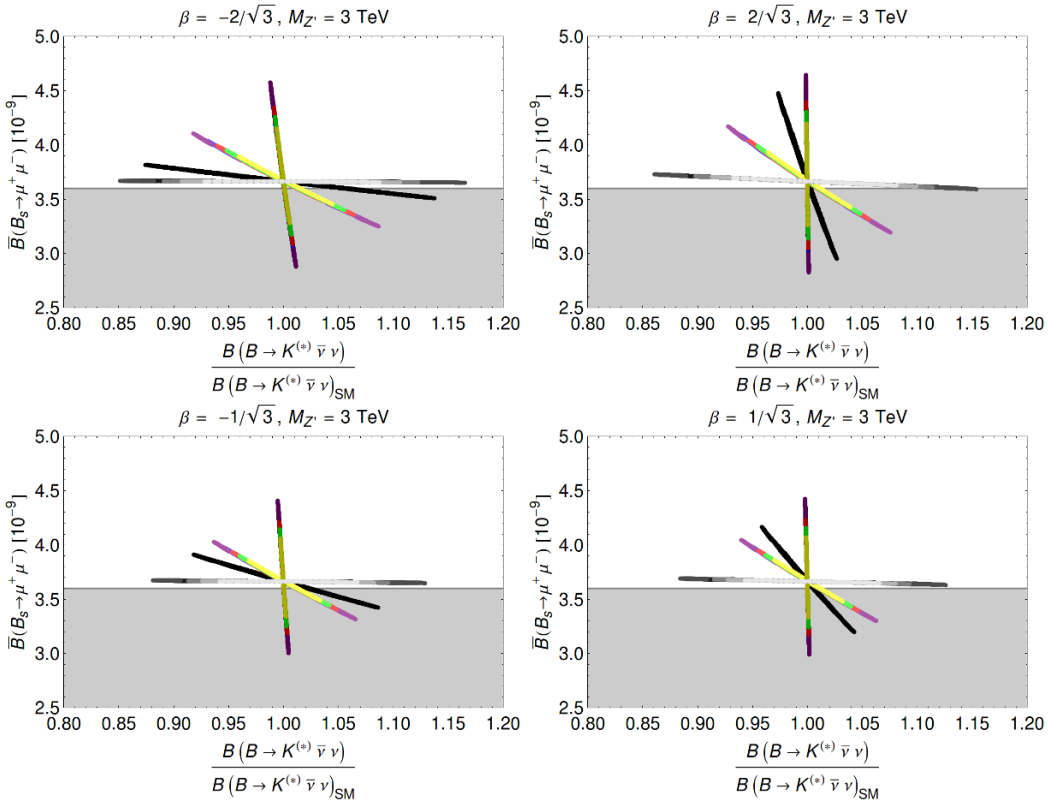

Figure 4. $\overline{\mathcal{B}}(B_s \to \mu^+\mu^-)$ versus the ratio $\mathcal{B}(B \to K\nu\bar{\nu})/\mathcal{B}(B \to K\nu\bar{\nu})_{\rm SM}$ for all four $\beta = \pm\frac{2}{\sqrt{3}}, \pm\frac{1}{\sqrt{3}}$. Colours as in figure 2.

- Finally we show the results for the four different values β in question and the fermion representations F_1 and F_2.

The results of this extensive numerical analysis are shown in figures 2–6. While with the comments just made these figures are self-explanatory, we would like to emphasize the most interesting features in them:

- Comparison of figures 2 and 3 demonstrates the breakdown of the invariance under (2.16) by $Z - Z'$ mixing. As seen in figures 4 and 5 this breakdown is even larger when channels with neutrinos in the final state are considered.

- From the present perspective, ignoring at first the constraints from electroweak precision observables, the most interesting model is the one with $\beta = -2/\sqrt{3}$ and fermion representations F_1 considered also by us in [4]. It allows to bring the theory closer to the data on $B_d \to K^*\mu^+\mu^-$ and $B_s \to \mu^+\mu^-$ than it is possible in the remaining models. In particular the inclusion of Z boson contributions allows to suppress $\overline{\mathcal{B}}(B_s \to \mu^+\mu^-)$ by $(15-20)\%$ below its SM value, which is not possible if only Z' contributions are present. But this suppression is only significant for $\tan\bar{\beta} > 1.0$ and is clearly visible for $\tan\bar{\beta} = 5.0$. On the other hand for $\tan\bar{\beta} = 0.2$ there is a destruc-

JHEP08(2014)039

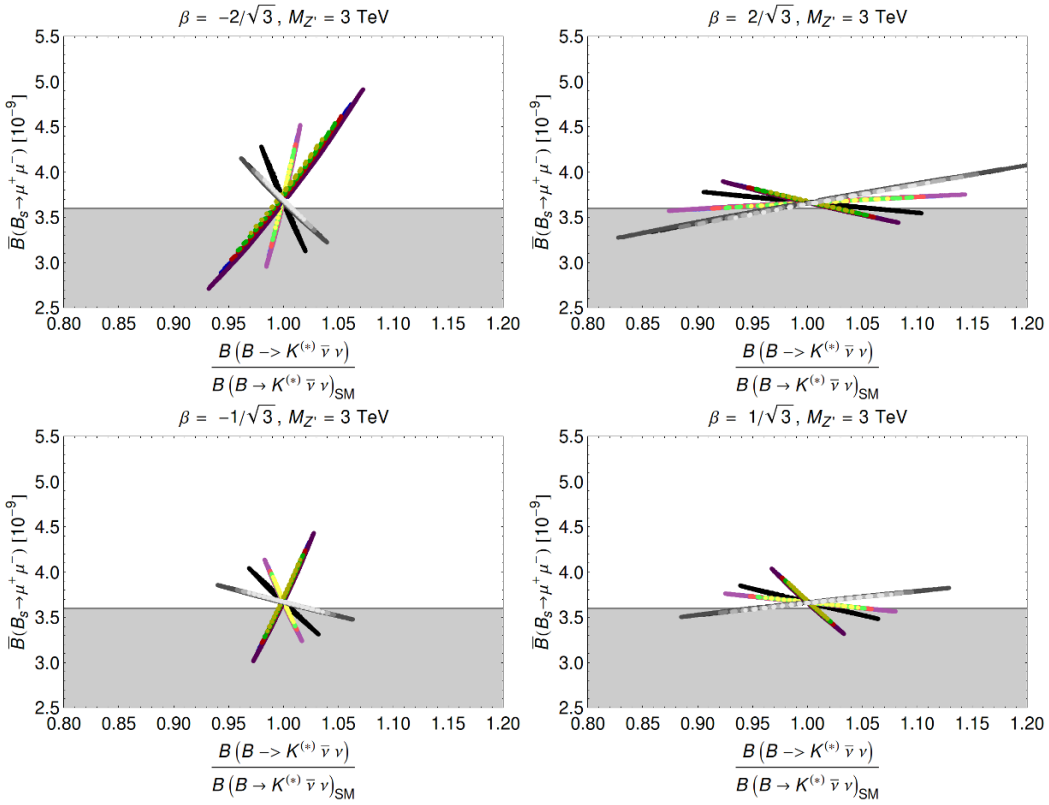

Figure 5. As in figure 4 but for F2.

tive interference between Z and Z' so that in this case NP effects in $\overline{\mathcal{B}}(B_s \to \mu^+\mu^-)$ turn out to be small.

- On the other hand if $B_d \to K^*\mu^+\mu^-$ anomaly disappeared but future more precise data would definitely show that $\overline{\mathcal{B}}(B_s \to \mu^+\mu^-)$ is significantly below its SM value, other models, in particular the one with $\beta = -2/\sqrt{3}$ but fermion representations F_2, would be favoured. Further tests would come from future measurements of decays with neutrinos in the final state.

- As seen in figures 4 and 5 in the case of neutrinos in the final state the dependence on $\tan\bar{\beta}$ is opposite to the case of $B_{s,d} \to \mu^+\mu^-$ and Z and Z' contributions interfere constructively for small $\tan\bar{\beta}$ but for large $\tan\bar{\beta}$ they cancel each other to a large extent.

- There is no specific correlations between the branching ratios for $B_s \to \mu^+\mu^-$ and $B_d \to \mu^+\mu^-$ decays and this implies significant departures from CMFV relation between their branching ratios. We show as an example in figure 6 the results for values of $\tan\bar{\beta} = 1,\ 5,\ 0.2$ and fermion representations F_1. The case without $Z - Z'$ mixing, that is pure Z' contributions, represented by the black regions allows to see that the presence of Z boson contributions in both decays represented by departure from these areas can be significant as could be deduced from previous results.

JHEP08(2014)039

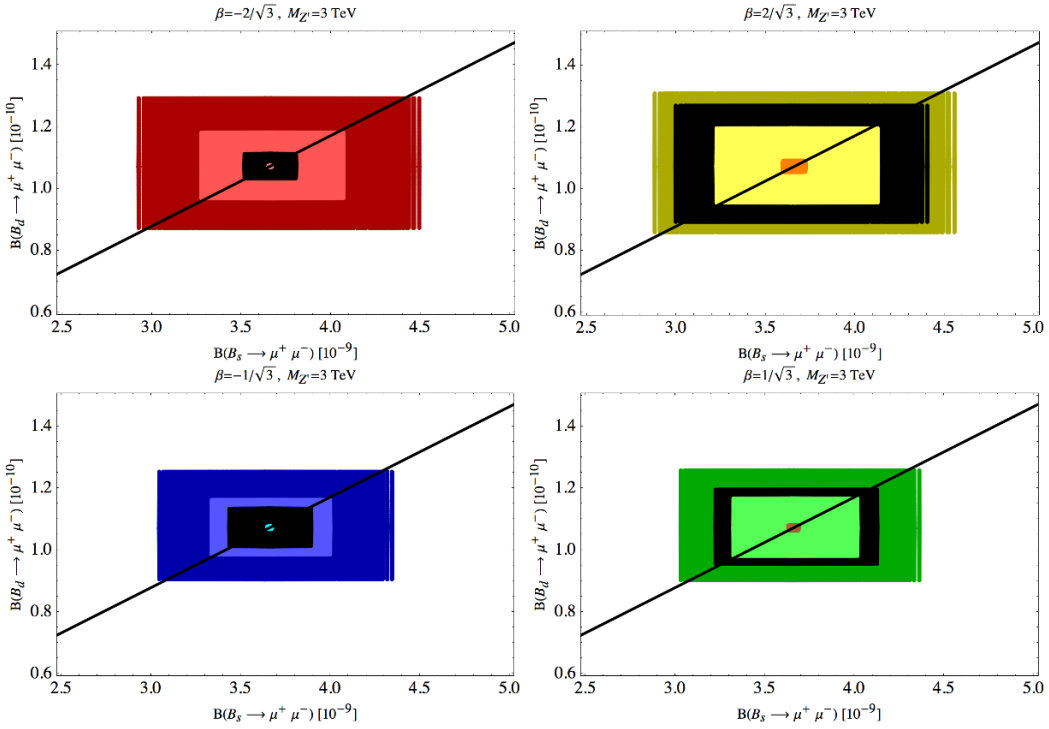

Figure 6. Correlation $\mathcal{B}(B_d \to \mu^+\mu^-)$ versus $\overline{\mathcal{B}}(B_s \to \mu^+\mu^-)$, without $Z - Z'$ mixing (black), $\tan\bar{\beta} = 1$ (lighter colours), $\tan\bar{\beta} = 5$ (darker colours) and $\tan\bar{\beta} = 0.2$ (small coloured box in the middle). The black line corresponds to the correlation in CMFV.

- As seen in figure 7 Z boson contributions have significant effect on the size of CP violation in $B_s \to \mu^+\mu^-$ that originates from a non-vanishing imaginary part of C_{10}^{NP}, in constrast to C_{10}^{SM} that is real. As the tests of CP-violating effects in this decay are in the distant future we only show the results for F_1 in this case.

Finally, we look at the $B_d \to K\mu^+\mu^-$ decay and its correlation with $\mathrm{Re}(\mathrm{C}_9^{\mathrm{NP}})$. The interest in the analysis of this decay lies in the fact that in contrast to $B_s \to \mu^+\mu^-$ and $B_d \to K^*\mu^+\mu^-$ that in 331 models are sensitive only to C_{10}^{NP} and C_9^{NP}, respectively, the branching ratio for $B_d \to K\mu^+\mu^-$ depends on both coefficients. Moreover, lattice calculations of the relevant form factors are making significant progress here [35, 36] and the importance of this decay will increase in the future.

Neglecting the interference between NP contributions the formula for the differential branching ratio confined to large q^2 region ($15\,\mathrm{GeV}^2 \leq q^2 \leq 22\,\mathrm{GeV}^2$)[4] reduces in 331 models in units of $1/\,\mathrm{GeV}^2$ to

$$10^9 \times \frac{d\mathcal{B}(B_d \to K\mu^+\mu^-)_{[15,22]}}{dq^2} = 13.1 + 3.15\ \mathrm{Re}(\mathrm{C}_9^{\mathrm{NP}}) - 3.23\mathrm{Re}(\mathrm{C}_{10}^{\mathrm{NP}}), \tag{3.10}$$

The relevant Wilson coefficients are given in (3.6) and (3.7). This formula describes triple correlation between $B_d \to K\mu^+\mu^-$, $\mathrm{Re}(\mathrm{C}_9^{\mathrm{NP}})$ and $\overline{\mathcal{B}}(B_s \to \mu^+\mu^-)$ which constitutes an

[4]This formula is based on [33] and a recent update. Straub, private communication.

JHEP08(2014)039

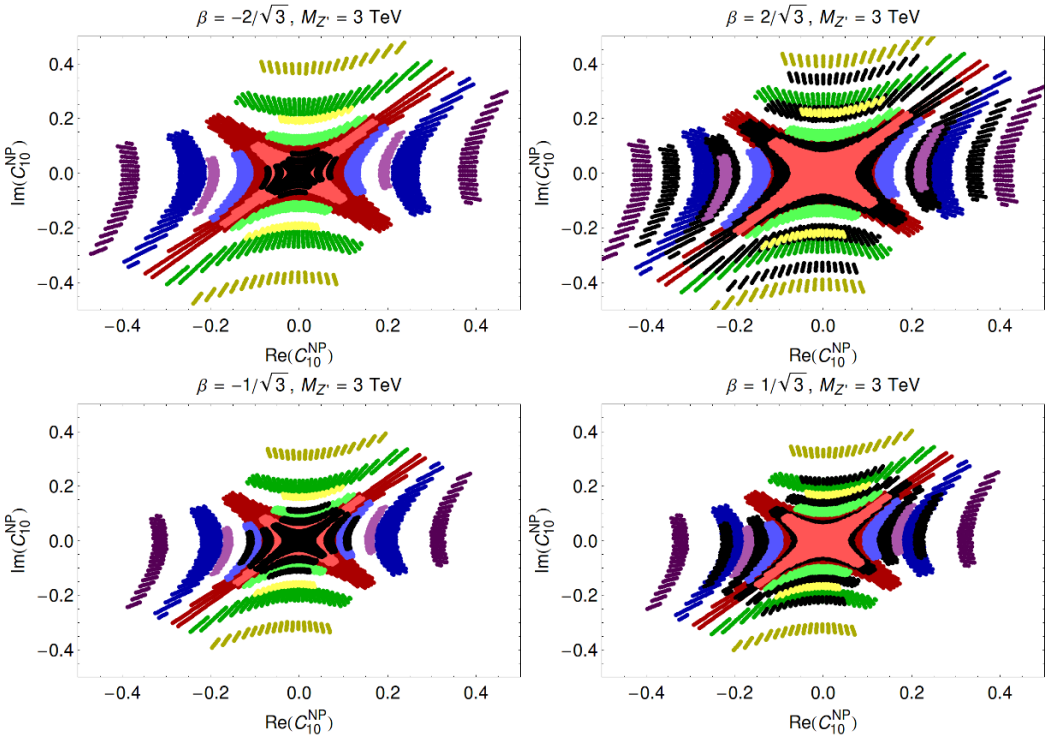

Figure 7. $\mathrm{Im}(\mathrm{C}_{10}^{\mathrm{NP}})$ versus $\mathrm{Re}(\mathrm{C}_{10}^{\mathrm{NP}})$ for $\beta = \pm 1/\sqrt{3}$ and $\beta = \pm 2/\sqrt{3}$ setting $M_{Z'} = 3\,\mathrm{TeV}$. Colour coding as in figure 2 but without $\tan\bar{\beta} = 0.2$ for which NP effects are very small.

important test for the models in question. In the absence of $Z - Z'$ mixing this triple correlation involving the rate for $B_d \to K\mu^+\mu^-$ at large q^2 can be found in figure 13 in [4] for the case of F_1 representations.

The error on the first SM term is estimated to be 10% [35, 36]. This should be compared with the LHCb result [37]

$$10^9 \times \frac{d\mathcal{B}(B_d \to K\mu^+\mu^-)_{[15,22]}}{dq^2} = 12.1 \pm 0.4 \pm 0.6 \qquad \text{(LHCb)}. \tag{3.11}$$

In figure 8 we generalize this result to include $Z - Z'$ mixing and in figure 9 we present corresponding results for F_2. As in the case of figures 2 and 3 we obtain straight lines with slopes depending on the values of β and $\tan\bar{\beta}$. The case of no $Z - Z'$ mixing is again shown by black lines. In these plots the colour coding is:

$$\tan\bar{\beta} = 1.0 \text{ (red)}, \quad \tan\bar{\beta} = 5.0 \text{ (blue)}, \quad \tan\bar{\beta} = 0.2 \text{ (green)}, \tag{3.12}$$

with lighter colours showing when $\overline{\mathcal{B}}(B_s \to \mu^+\mu^-)$ is enhanced and with darker ones when it is suppressed with respect to the SM prediction.

There are two striking differences between these results an those in figures 2–5. The effects of $Z - Z'$ mixing in figures 8 and 9 are significantly smaller and consequently the symmetry in (2.16) is less broken.

At this point we would like to emphasize that all the results described until now do not take into account the constraints from electroweak precision tests. In section 5 we will

JHEP08(2014)039

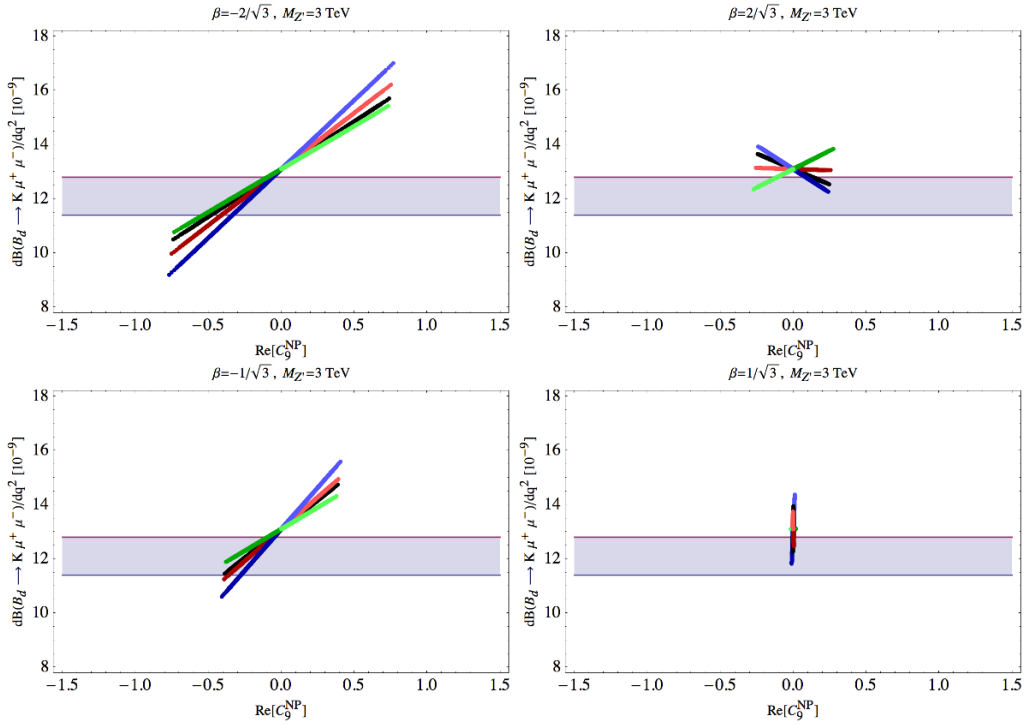

Figure 8. Correlation of the differential branching ratio for $B_d \to K\mu^+\mu^-)_{[15,22]}$ versus $\mathrm{Re}(\mathrm{C}_9^{\mathrm{NP}})$ for $\beta = \pm 1/\sqrt{3}$ and $\beta = \pm 2/\sqrt{3}$ and F_1 setting $M_{Z'} = 3\,\mathrm{TeV}$ and different values of $\tan\bar{\beta}$ with colour coding given in (3.12). $\overline{\mathcal{B}}(B_s \to \mu^+\mu^-) \leq \overline{\mathcal{B}}(B_s \to \mu^+\mu^-)_{\mathrm{SM}}$ (darker colours) and $\overline{\mathcal{B}}(B_s \to \mu^+\mu^-) \geq \overline{\mathcal{B}}(B_s \to \mu^+\mu^-)_{\mathrm{SM}}$ (lighter colours) . The gray regions show the experimental range in (3.11).

analyze which lines in figures 2–5, 8 and 9 survive the latter tests and which not. In any case with $M_{Z'} = 3\,\mathrm{TeV}$, as demonstrated in [4], the bounds from LEP-II and LHC are satisied.

3.3 Numerical results for rare K decays

In our recent paper [38] we have reemphasized the strong dependence of rare K decay branching ratios on the values of the elements of the CKM matrix $|V_{ub}|$ and $|V_{cb}|$. This dependence is particularly strong in the case of $K_L \to \pi^0\nu\bar{\nu}$ as seen in table 3 of that paper. While in [38] we have studied six scenarios for $|V_{ub}|$ and $|V_{cb}|$ in 331 models most of these scenarios are ruled out by ε_K. In fact as already pointed out in [3] NP effects in ε_K are rather small when constraints from $B^0_{d,s} - \bar{B}_{d,s}$ mixing are taken into account. Therefore the 331 models can only be made consistent with data on ε_K for values of $|V_{ub}|$ and $|V_{cb}|$ for which the SM prediction for ε_K is rather close to this data. Then only scenarios d) and f) in [38]

$$d) \qquad |V_{ub}| = 4.1 \times 10^{-3} \qquad |V_{cb}| = 42.0 \times 10^{-3} \tag{3.13}$$

$$f) \qquad |V_{ub}| = 3.9 \times 10^{-3} \qquad |V_{cb}| = 42.0 \times 10^{-3} \tag{3.14}$$

survive the ε_K constraint in 331 models as then for central values of remaining parameters $|\varepsilon_K| = 2.35 \times 10^{-3}$ and $|\varepsilon_K| = 2.25 \times 10^{-3}$, respectively. This is close to the experimental value $|\varepsilon_K| = 2.23 \times 10^{-3}$ so that there is no problem in fitting the data.

JHEP08(2014)039

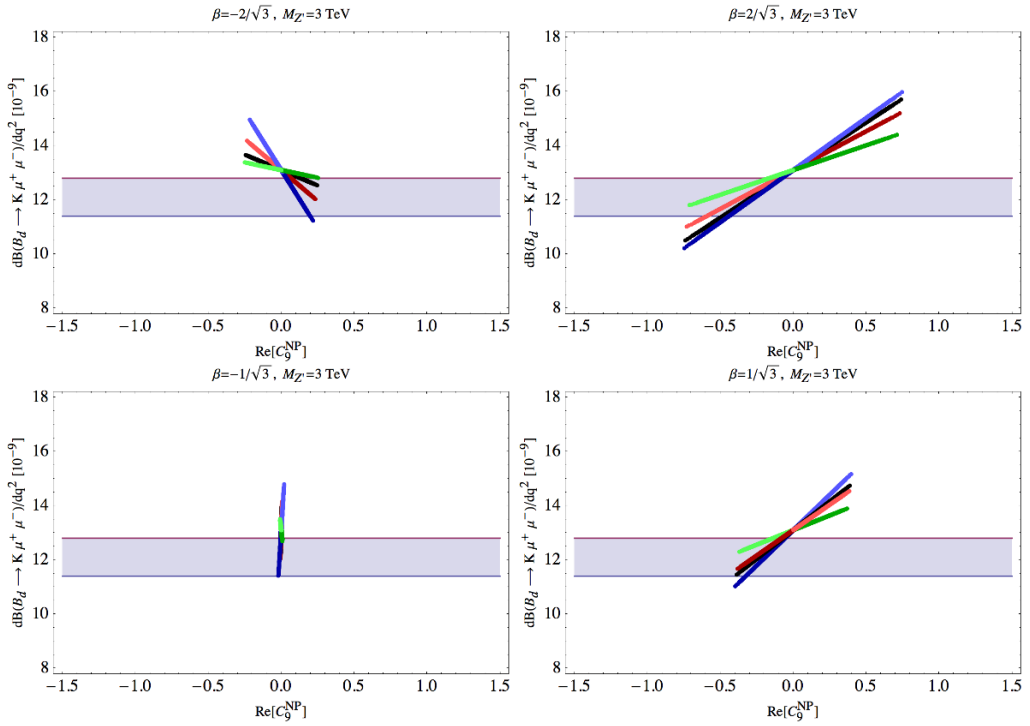

Figure 9. As in figure 8 but for F_2.

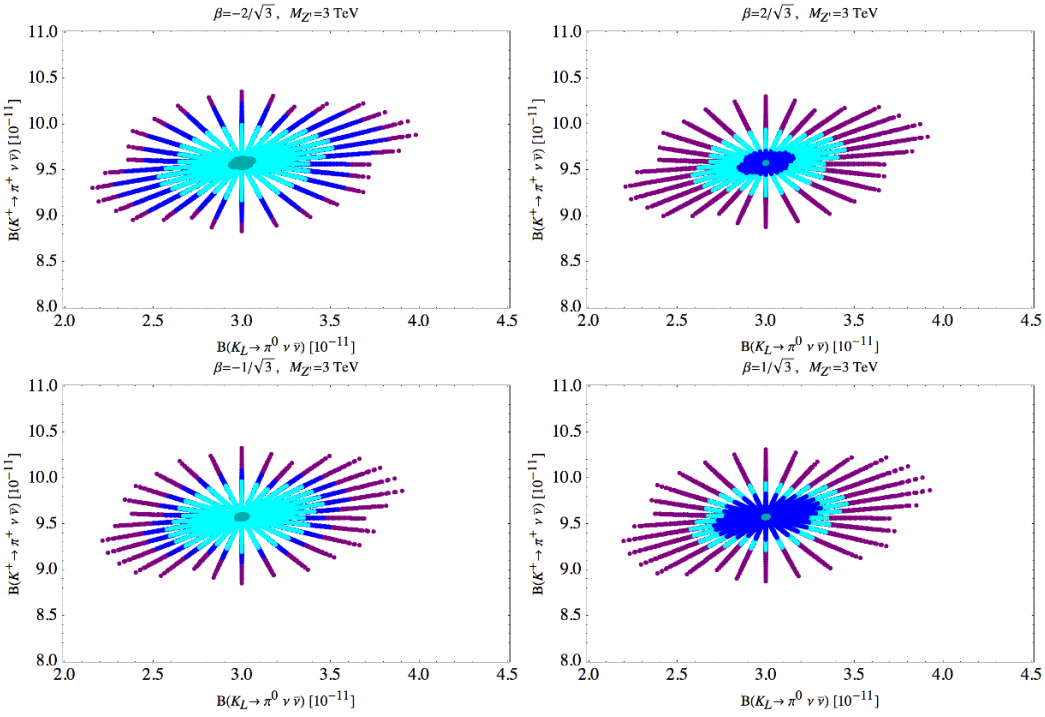

Figure 10. $K^+ \to \pi^+ \nu\bar{\nu}$ versus $K_L \to \pi^0 \nu\bar{\nu}$ for different values of β for $\tan\bar{\beta} = 1.0$ (cyan), $\tan\bar{\beta} = 5.0$ (darker cyan), $\tan\bar{\beta} = 0.2$ (purple) and without $Z - Z'$ mixing (blue) for F_1 representations.

JHEP08(2014)039

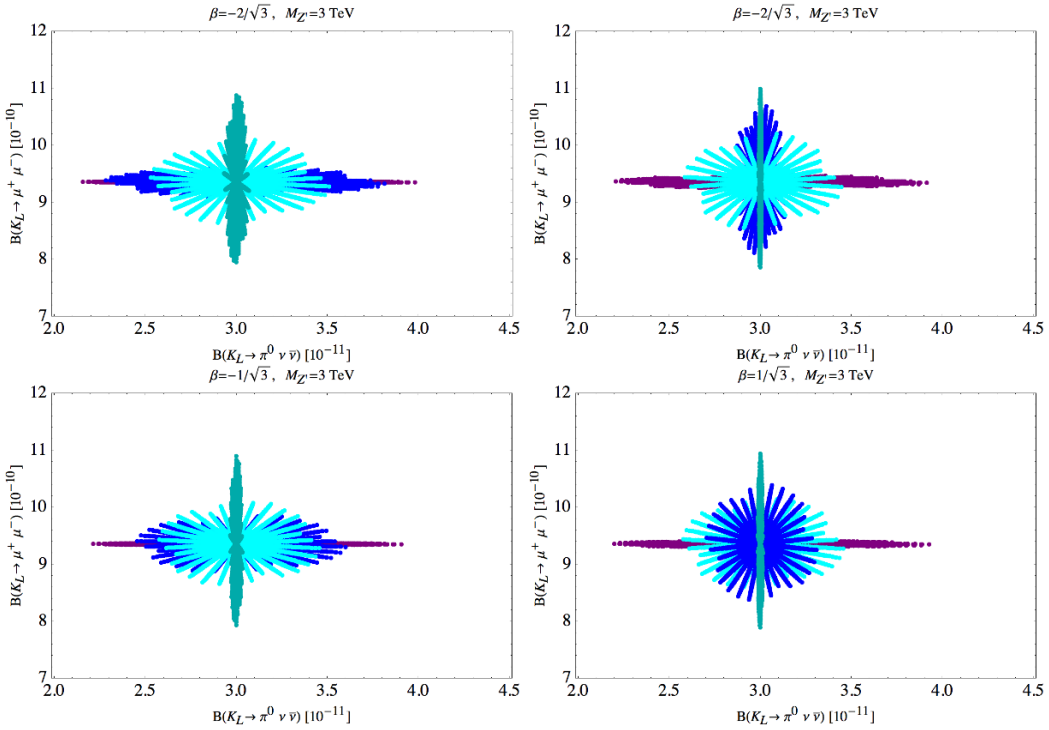

Figure 11. $\mathcal{B}(K_L \to \mu^+\mu^-)$ versus $K_L \to \pi^0\nu\bar{\nu}$ for different values of β for $\tan\bar{\beta} = 1.0$ (cyan), $\tan\bar{\beta} = 5.0$ (darker cyan), $\tan\bar{\beta} = 0.2$ (purple) and without $Z - Z'$ mixing (blue) for F_1 representations.

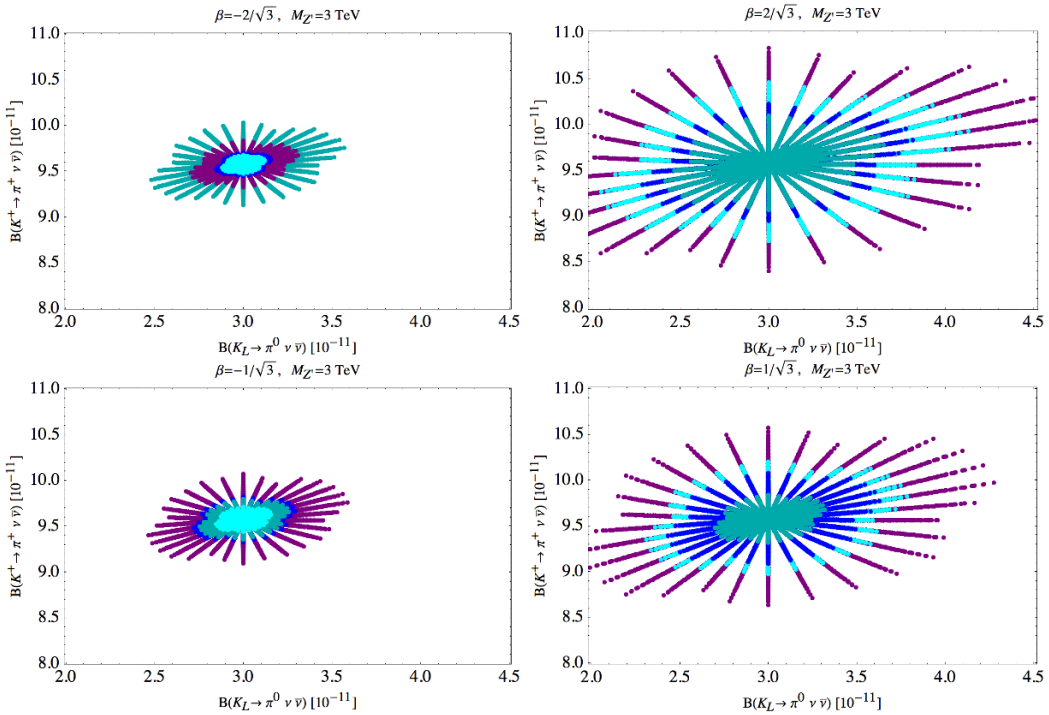

Figure 12. $K^+ \to \pi^+\nu\bar{\nu}$ versus $K_L \to \pi^0\nu\bar{\nu}$ as in figure 11 but for F2.

JHEP08(2014)039

Now in [4] and in the analysis of B decays in the present paper we have used the values

$$|V_{ub}| = 3.6 \times 10^{-3} \qquad |V_{cb}| = 42.4 \times 10^{-3} \tag{3.15}$$

which implies $|\varepsilon_K| = 2.17 \times 10^{-3}$ that is rather close to the choice f) above and as it also allows to satisfy the ε_K constraint, we will use these values for rare K decays and ε'/ε.

In figures 10 and 11 we show various correlations between rare decay branching ratios for the four 331 models considered for the F_1 case, three values of $\tan\bar{\beta} = 1, 5, 0.2$ and the case without $Z - Z'$ mixing which represents sole Z' contributions. While these plots are self-explanatory, in particular when considered simultaneously with table 1, we would like to emphasize a number of most important features in them. These are:

- A rather striking feature is the cancellation of Z' and Z contributions to the branching ratios for $K^+ \to \pi^+\nu\bar{\nu}$ and $K_L \to \pi^0\nu\bar{\nu}$ for $\tan\bar{\beta} = 5.0$ so that in this case one obtains basically the SM prediction independently of the value of β. On the contrary in the case of $K_L \to \mu^+\mu^-$ for $\tan\bar{\beta} = 5.0$ and in particular for negative β NP effects are enhanced through $Z - Z'$ mixing. This difference between decays with neutrino and muons in the final state has been also seen in the case of B decays.

- A different behaviour is observed for $\tan\bar{\beta} = 1.0$. In the case of $K^+ \to \pi^+\nu\bar{\nu}$ and $K_L \to \pi^0\nu\bar{\nu}$ for models with $\beta = -2/\sqrt{3}$ and $\beta = -1/\sqrt{3}$ there is a *destructive* interference between Z and Z' contributions decreasing somewhat NP effects due to Z' exchange alone. For $\beta = 2/\sqrt{3}$ and $\beta = 1/\sqrt{3}$, on the other hand, the corresponding interference is *constructive* and NP effects are increased. On the contrary the effects of $Z - Z'$ mixing for $\tan\bar{\beta} = 1.0$ in $K_L \to \mu^+\mu^-$ are rather small.

- For $\tan\bar{\beta} = 0.2$ NP effects in $K_L \to \pi^0\nu\bar{\nu}$ and $K^+ \to \pi^+\nu\bar{\nu}$ increase but they basically disappear in the case $K_L \to \mu^+\mu^-$.

- On the whole NP effects except for the case of $K_L \to \pi^0\nu\bar{\nu}$ and $\tan\bar{\beta} \leq 1$ are rather small and it will be difficult to distinguish them from SM expectations unless parametric uncertainties decrease by much and experimental data will be very precise.

Considering the case of F_2 representations one can deduce from table 2 that the symmetry in (2.16) is significantly broken in rare K decays but the size of NP effects is similar to the F_1 case. As an example we show in figure 12 the correlation between the branching ratios for $K^+ \to \pi^+\nu\bar{\nu}$ and $K_L \to \pi^0\nu\bar{\nu}$ for F_2. In particular for $\beta = 2/\sqrt{3}$ and $\tan\bar{\beta} = 0.2$ NP effects are significant.

But the main message from our analysis of rare B and K decays is that neglecting Z contributions in decays governed by axial vector couplings to muons or left-handed couplings to neutrinos is not justified and observing significant NP effects in $B_{s,d} \to \mu^+\mu^-$ would imply $\tan\bar{\beta} > 1$ and only small effects in $K_L \to \pi^0\nu\bar{\nu}$ and $K^+ \to \pi^+\nu\bar{\nu}$. On the other hand confirming SM predictions for $B_{s,d} \to \mu^+\mu^-$ to high degree would in 331 models for $M_{Z'} = 3\,\text{TeV}$ still allow for modest by significant departures from SM expectations for these decays and imply for 331 models $\tan\bar{\beta} \leq 1$.

JHEP08(2014)039

Again the results just described do not take into account the constraints from electroweak precision tests and it will be interesting to see in section 5 the impact of the latter tests on them.

4 The ratio ε'/ε

4.1 Preliminaries

Recently we have presented a new analysis of ε'/ε within the SM and models with tree-level Z' and Z boson exchanges [38]. Several of the formulae presented in that paper can be directly used in the context of the 331 models and consequently our presentation will be rather brief. In 331 models we have

$$\left(\frac{\varepsilon'}{\varepsilon}\right)_{331} = \left(\frac{\varepsilon'}{\varepsilon}\right)_{\rm SM} + \left(\frac{\varepsilon'}{\varepsilon}\right)_{Z} + \left(\frac{\varepsilon'}{\varepsilon}\right)_{Z'}, \tag{4.1}$$

where the formula for the SM contribution, an update of the original one in [39], is given in (53) of [38].

4.2 Z contribution

This case is simple as the only thing to be done is to introduce shifts in the functions X, Y and Z that enter the SM model contribution to ε'/ε. Using the results of section 7 in [38] together with the relation (2.2) we find

$$\Delta X = \Delta Y = \Delta Z = \sin\xi\, c_W \frac{8\pi^2}{g^3} \frac{{\rm Im}\Delta_L^{sd}(Z')}{{\rm Im}\lambda_t} \tag{4.2}$$

where $g = 0.652$ and $\lambda_t = V_{td}V_{ts}^*$. Replacing then the functions $X_0(x_t)$, $Y_0(x_t)$ and $Z_0(x_t)$ by

$$X = X_0(x_t) + \Delta X, \qquad Y = Y_0(x_t) + \Delta Y, \qquad Z = Z_0(x_t) + \Delta Z \tag{4.3}$$

in the formula (53) for ε'/ε in [38] allows to take automatically the first two contributions in (4.1) in 331 models into account.

4.3 Z' contribution

Using the general formulae for the flavour diagonal Z' couplings to quarks in [3, 4] we find that in LO as far as penguin operators are concerned the only non-vanishing Wilson coefficients at $\mu = M_{Z'}$ are the ones of the known QCD penguin operator Q_3, the known electroweak penguin operator Q_7 as well as of the operator

$$\tilde{Q}_3 = (\bar{s}d)_{V-A}\left[(\bar{b}b)_{V-A} + (\bar{t}t)_{V-A}\right] \tag{4.4}$$

which is present due to different couplings of Z' to the third generation of quarks. Their coefficients are given in 331 models as follows

$$C_3(M_{Z'}) = \frac{g}{2\sqrt{3}c_W}\sqrt{f(\beta)}\left[-1 + \left(1 + \frac{\beta}{\sqrt{3}}\right)s_W^2\right]\frac{\Delta_L^{sd}(Z')}{4M_{Z'}^2} \tag{4.5}$$

JHEP08(2014)039

$$C_7(M_{Z'}) = \frac{g}{2\sqrt{3}c_W}\sqrt{f(\beta)}\frac{4}{\sqrt{3}}\beta s_W^2\frac{\Delta_L^{sd}(Z')}{4M_{Z'}^2} \tag{4.6}$$

$$\tilde{C}_3(M_{Z'}) = \frac{g}{2\sqrt{3}c_W}\sqrt{f(\beta)}\left[2c_W^2\right]\frac{\Delta_L^{sd}(Z')}{4M_{Z'}^2} \tag{4.7}$$

with $f(\beta)$ defined in (2.10). We recall that these results are valid for fermion representation F_1. For F_2 one just has to reverse the sign in front of β according to the rules outlined in section 2.2.

The coefficients of these three operators at $\mu = M_{Z'}$ are of the same order. Yet, when QCD renormalization group effects are included and the size of hadronic matrix elements relevant for ε'/ε are taken into account we find that the Q_3 and $\tilde{Q}_3$ contributions can be neglected leaving the left-right electroweak penguin operators

$$Q_7 = \frac{3}{2}(\bar{s}d)_{V-A}\sum_{q=u,d,s,c,b,t} e_q\,(\bar{q}q)_{V+A} \qquad Q_8 = \frac{3}{2}(\bar{s}_\alpha d_\beta)_{V-A}\sum_{q=u,d,s,c,b,t} e_q(\bar{q}_\beta q_\alpha)_{V+A} \tag{4.8}$$

as the only relevant operators in Z' contribution to ε'/ε in 331 models. However, even if at LO the Wilson coefficient of Q_8 vanishes at $\mu = M_{Z'}$, at $\mu = m_c$ used in our numerical analysis of ε'/ε its Wilson coefficient $C_8(m_c)$ is of the same order as $C_7(m_c)$. Indeed the relevant one-loop anomalous dimension matrix in the (Q_7, Q_8) basis is given by

$$\hat{\gamma}_s^{(0)} = \begin{pmatrix} 2 & -6 \\ 0 & -16 \end{pmatrix}. \tag{4.9}$$

Performing the renormalization group evolution from $M_{Z'}$ to $m_c = 1.3\,\text{GeV}$ we find using explicit formulae in [38]

$$C_7(m_c) = 0.82\,C_7(M_{Z'}) \qquad C_8(m_c) = 1.35\,C_7(M_{Z'}). \tag{4.10}$$

Due to the large element $(1,2)$ in the matrix (4.9) and the large anomalous dimension of the Q_8 operator represented by the $(2,2)$ element in (4.9), the two coefficients are comparable in size. But the matrix element $\langle Q_7\rangle_2$ is colour suppressed which is not the case of $\langle Q_8\rangle_2$ and within a good approximation we can neglect the contributions of Q_7. In summary, it is sufficient to keep only Q_8 contributions in ε'/ε in 331 models.

The relevant isospin amplitude A_2 in $K \to \pi\pi$ decays necessary to calculate Z' contribution to ε'/ε is given as follows

$$A_2^{\text{NP}} = C_8(m_c)\langle Q_8(m_c)\rangle_2 \tag{4.11}$$

where [38]

$$\langle Q_8(m_c)\rangle_2 = 0.57\left[\frac{114\,\text{MeV}}{m_s(m_c)+m_d(m_c)}\right]^2\left[\frac{B_8^{(3/2)}}{0.65}\right]\text{GeV}^3 \tag{4.12}$$

with $B_8^{(3/2)} = 0.65 \pm 0.05$ from lattice QCD [40].

JHEP08(2014)039

In our numerical analysis we will use for the quark masses the values from FLAG 2013 [41]

$$m_s(2\,\text{GeV}) = (93.8 \pm 2.4)\,\text{MeV}, \qquad m_d(2\,\text{GeV}) = (4.68 \pm 0.16)\,\text{MeV}. \tag{4.13}$$

Then at the nominal value $\mu = m_c = 1.3\,\text{GeV}$ we have

$$m_s(m_c) = (108.6 \pm 2.8)\,\text{MeV}, \qquad m_d(m_c) = (5.42 \pm 0.18)\,\text{MeV}. \tag{4.14}$$

The final expression for Z' contributions is given by

$$\left(\frac{\varepsilon'}{\varepsilon}\right)_{Z'} = \frac{\omega_+}{|\varepsilon_K|\sqrt{2}} \frac{\text{Im}A_2^{\text{NP}}}{\text{Re}A_2} \tag{4.15}$$

where [42]

$$\omega_+ = (4.1 \pm 0.1) \times 10^{-2}\,. \tag{4.16}$$

In evaluating (4.15) we use, as in the case of the SM, the experimental values for $\text{Re}A_2$ and ε_K:

$$\text{Re}A_2 = 1.210(2) \times 10^{-8}\ \text{GeV}, \qquad |\varepsilon_K| = 2.228(11) \times 10^{-3}\,. \tag{4.17}$$

As NP contributions to ε'/ε, both due to Z and Z', are dominated by the operator Q_8, the ratio of these contributions depends with high accuracy simply on the ratio of $C_8(m_c)$ in these two contributions. This allows then to derive a simple relation

$$\left(\frac{\varepsilon'}{\varepsilon}\right)_{Z} = R_{\varepsilon'} \left(\frac{\varepsilon'}{\varepsilon}\right)_{Z'}, \tag{4.18}$$

where ($s_W^2 = 0.23116$)

$$R_{\varepsilon'} = -\frac{0.53}{\beta}\,\frac{c_W^2}{3}\left[3\beta\frac{s_W^2}{c_W^2} + \sqrt{3}a\right] = -\frac{0.14}{\beta}\,\left[0.90\beta + \sqrt{3}a\right]. \tag{4.19}$$

This expression is valid for fermion representation F_1. For F_2 for a given β one should just remove the overall minus sign in this expression as the β in front of the parenthesis enters the Z' coupling. The expression in the parenthesis comes from $Z - Z'$ mixing and is independent of the fermion representation. The factor 0.53 summarizes the difference in renormalization group effects for Z and Z' contributions. QCD renormalization of Q_8 gives alone 0.56 and additional small suppression comes from the running of electroweak parameters. We list the values of $R_{\varepsilon'}$ in the last row of tables 1–3. Evidently Z' dominates NP contributions to ε'/ε implying that $Z - Z'$ mixing effects are small in this ratio. The two exceptions are the case of $\beta = -1/\sqrt{3}$ and $\tan\bar{\beta} = 5$ and the case of $\beta = 1/\sqrt{3}$ and $\tan\bar{\beta} = 0.2$ for which Z contribution reaches 50% of the Z' one.

4.4 Numerical analysis of ε'/ε

In figure 13 we show ε'/ε versus ε_K. We make the following observations:

- 331 models for all values of β are consistent with the data for ε'/ε provided $B_6^{(1/2)} \approx 1.0$ represented by *red* colour.

JHEP08(2014)039

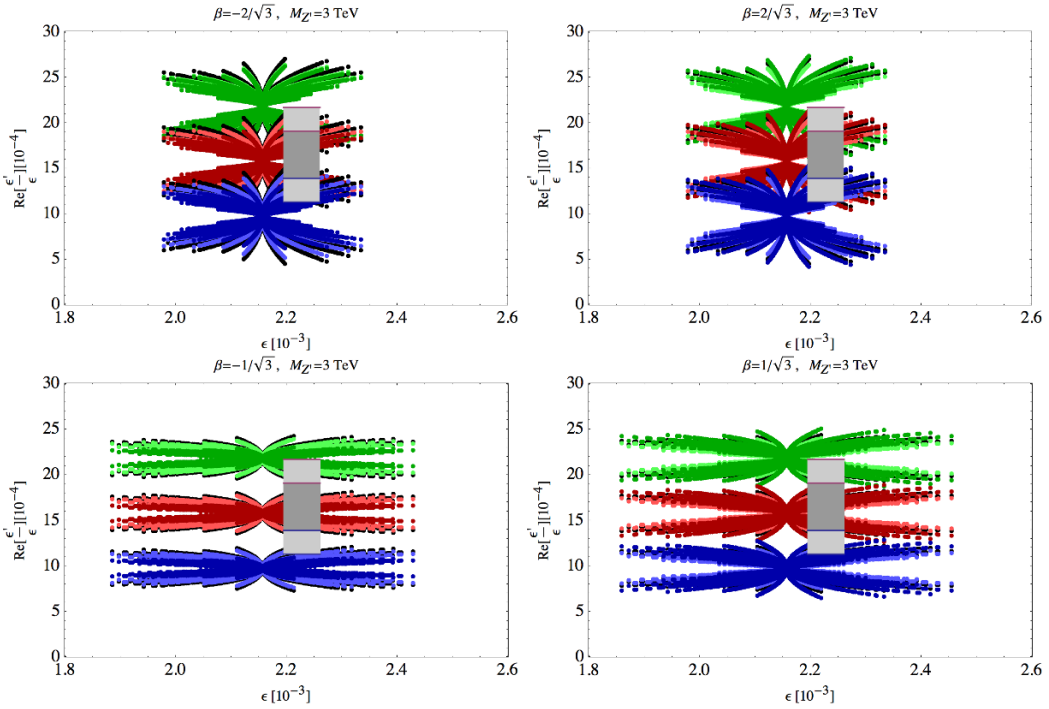

Figure 13. ε'/ε versus ε_K, $M_{Z'} = 3$ TeV, F_1 representations, different values of $\beta = \pm\frac{2}{\sqrt{3}}, \pm\frac{1}{\sqrt{3}}$, $\tan\bar{\beta} = 1(5)$ lighter colours (darker colours) and no $Z - Z'$ mixing (black) and $B_6^{(1/2)} = 0.75$ (blue), $B_6^{(1/2)} = 1.00$ (red), $B_6^{(1/2)} = 1.25$ (green). (Light) gray area: $1\sigma(2\sigma)$ range of ε'/ε and 3σ range of ε_K.

- $Z - Z'$ mixing effects are for most parameters small as already expected on the basis of the formula (4.19) and the values of $R_{\varepsilon'}$ in tables 1–3.

In figure 14 we show ε'/ε versus $\mathcal{B}(K_L \to \pi^0\nu\bar{\nu})$ for fermion representations F_1. We observe that the correlation between these two observables is very strict as ε'/ε is linear in the imaginary parts of the flavour violating Z' and Z couplings and NP contribution to $\mathcal{B}(K_L \to \pi^0\nu\bar{\nu})$ is dominated by the interference of the SM and NP amplitude. Consequently is also linear in these couplings. Two interesting features of these plots should be emphasized

- while for *negative* β the ratio ε'/ε decreases with increasing $\mathcal{B}(K_L \to \pi^0\nu\bar{\nu})$, for *positive* β it increases with increasing $\mathcal{B}(K_L \to \pi^0\nu\bar{\nu})$. The latter property is rather rarly found in other extensions of the SM.

- The effects of $Z - Z'$ mixing are clearly visible, in particular for $\beta > 0$. They originate dominantly in the ones present in $K_L \to \pi^0\nu\bar{\nu}$.

- As already known from figure 13 the agreement of the theory and the data is best for $B_6^{(1/2)} \approx 1.0$.

JHEP08(2014)039

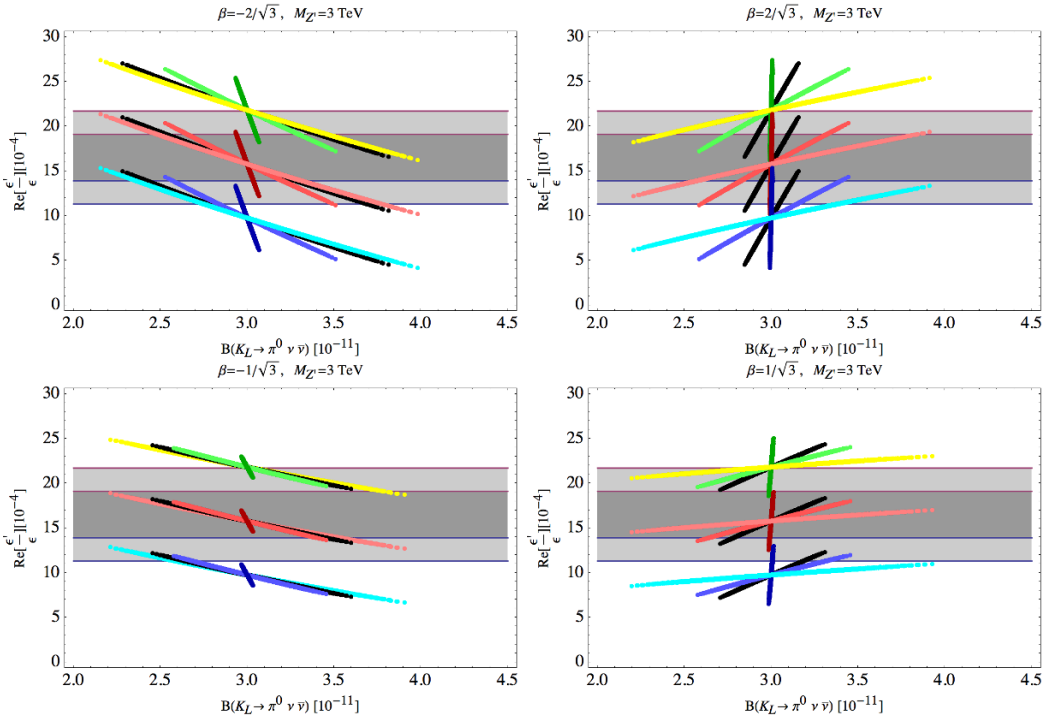

Figure 14. ε'/ε versus $\mathcal{B}(K_L \to \pi^0\nu\bar{\nu})$, $M_{Z'} = 3$ TeV, different values of $\beta = \pm\frac{2}{\sqrt{3}}, \pm\frac{1}{\sqrt{3}}$, different values of $B_6^{(1/2)} = 0.75,\ 1.00,\ 1.25$ and $\tan\bar{\beta} = 1$ (light blue, light red, light green), $\tan\bar{\beta} = 5$ (dark blue, dark red, dark green), $\tan\bar{\beta} = 0.2$ (cyan, pink, yellow) and no $Z - Z'$ mixing (black, black, black). Fermion representations F_1.

5 Electroweak precision observables

5.1 Preliminaries

The modifications of the Z boson couplings due to $Z - Z'$ mixing in 331 models can be tested through electroweak precision measurements at LEP-I and SLD and such an analysis can be found in [9] and recently in [43]. As our formula for $\sin\xi$ differs from the one used in these papers we want to analyze the impact of $Z-Z'$ mixing on most important electroweak precision observables (EWPO) and study their dependence on β, $\tan\bar{\beta}$ and the choice of fermion representations. Thus our next goal is to construct three tables for the shifts of a number of EWPO relative to SM predictions. This will eventually allow us to investigate the correlations between NP effects in EWPO and flavour observables. In these tables we will set $M_{Z'} = 3\,\text{TeV}$. As the shifts in question are inversely proportional to $M_{Z'}^2$ it is straight forward to find out what happens for other values of $M_{Z'}$.

Transparent analyses of the effects of $Z - Z'$ mixing in EWPO can be found in [29, 44, 45]. We will follow here the general analysis in [29] and to this end it is useful to note that our couplings of a given fermion f to Z and Z' differ from the couplings $v_{S,N}^f$ and $a_{S,N}^f$ used in that paper by an overall factor:

$$\Delta_V^{ff}(Z) = \frac{g}{\cos\theta_W} v_S^f, \qquad \Delta_A^{ff}(Z) = \frac{g}{\cos\theta_W} a_S^f, \tag{5.1}$$

JHEP08(2014)039

$$\Delta_V^{ff}(Z') = \frac{g}{\cos\theta_W} v_N^f, \qquad \Delta_A^{ff}(Z') = \frac{g}{\cos\theta_W} a_N^f \,. \tag{5.2}$$

For Z couplings we then have

$$v_S^f = T_{3L}^f - 2\sin^2\theta_W Q^f, \qquad a_S^f = -T_{3L}^f \tag{5.3}$$

where T_{3L}^f is the third component of the weak isospin of the fermion f and Q^f its electric charge. Our effective Z couplings in (2.6) are then related to the analogously defined ones in [29] simply as follows

$$[\Delta_V^f(Z)]_{\rm eff} = \frac{g}{\cos\theta_W} v_{\rm eff}^f, \qquad [\Delta_A^f(Z)]_{\rm eff} = \frac{g}{\cos\theta_W} a_{\rm eff}^f. \tag{5.4}$$

Due to the $Z - Z'$ mixing the ϱ parameter, defined by

$$\varrho = \frac{M_W^2}{M_Z^2 \cos^2\theta_W} \tag{5.5}$$

receives tree-level contribution $\Delta\varrho_M$ which for $M_{Z'} \gg M_Z$ is given by [29, 44, 45]

$$\Delta\varrho_M = \left(\frac{M_{Z'}^2}{M_Z^2}\right) \sin^2\xi \,. \tag{5.6}$$

This shift is strictly positive and $\mathcal{O}(M_Z^2/M_{Z'}^2)$. Consequently it is of the same order as the $Z - Z'$ mixing effects in the effective Z couplings in (2.6) so that it has to be taken into account. On the other hand we conclude on the basis of [46] that in 331 models studied by us the oblique contributions involving new heavy charged gauge bosons, scalars and fermions can be neglected when their masses are in the few TeV regime. Consequently the shift in $\Delta\varrho$ due to NP in these models is dominated by $\Delta\varrho_M$ given above.

Keeping fixed as input parameters $\alpha(M_Z)$, G_F and M_Z, the effective Weinberg angle in (5.5) is modified due to the shift in ϱ as follows [29, 44]

$$\Delta(\sin^2\theta_W) = -\kappa\Delta\varrho_M, \qquad \kappa = \frac{\sin^2\theta_W \cos^2\theta_W}{\cos^2 2\theta_W} \,. \tag{5.7}$$

It should be noted that this shift is strictly negative and this property is valid for any Z' model. Yet, as we will see below, this does not mean that the shift in the so-called effective $\sin^2\theta_{\rm eff}^l$ is negative in any Z' model as the contributions to Z couplings that are proportional to $\sin\xi$ are clearly model dependent. Some aspects of this dependence has been already analyzed in the context of 331 models in [43]. Our improved formula for $\sin\xi$ in (2.9) and the gained insight on the correlations between $Z - Z'$ mixing and FCNCs processes allows us to have another look at this issue thereby also generalizing the analysis in [43].

Next denoting a given observable by $\mathcal{O}$ the shift due to $Z - Z'$ mixing can be linearized in $\Delta\varrho_M$ and $\sin\xi$ as follows [29, 45]

$$\frac{\delta\mathcal{O}}{\mathcal{O}} = A_{\mathcal{O}}\Delta\varrho_M + B_{\mathcal{O}}\sin\xi \,. \tag{5.8}$$

JHEP08(2014)039

Here the coefficients $A_{\mathcal{O}}$ are universal and depend only on the SM parameters and couplings. On the other hand $B_{\mathcal{O}}$ depend on the diagonal Z'-couplings in (2.6). Direct Z' contributions to EWPO are negligible.

We will list the general formulae for the coefficients $A_{\mathcal{O}}$ and $B_{\mathcal{O}}$ below but rather then giving numerical values for them as done in [29] we will calculate the shifts in EWPO for different values of β, $\tan\bar{\beta}$ and the fermion representations F_1 and F_2 for $M_{Z'} = 3\,\text{TeV}$. To this end we will proceed as follows

- We will calculate a number of EWPO as functions of the effective diagonal Z-couplings in (2.6) in 331 models using tree-level formulae. In doing this one should remember that in addition to the direct contribution of Z' to the effective Z couplings leading to the second term in (5.8) also the shift in $\sin^2\theta_W$ entering the vector Z coupling has to be taken into account. That is in the Z coupling to a fermion f one should make additional replacement:

$$v_S^f \to v_S^f - 2\Delta(\sin^2\theta_W)Q^f = v_S^f + 2\kappa Q^f \Delta\varrho_M \tag{5.9}$$

  with $\Delta(\sin^2\theta_W)$ given in (5.7). This contribution to the shift $\delta\mathcal{O}$ is represented by the first term (5.8).

- Denoting the result for a given observable calculated in this manner by $\mathcal{O}(\xi)$ we can simply calculate the shift $\delta\mathcal{O}$ due to NP by subtracting the pure SM contributions at tree level:

$$\delta\mathcal{O}(\xi) = \mathcal{O}(\xi) - \mathcal{O}(0). \tag{5.10}$$

  As the mixing effects are very small the higher order terms generated by this numerical procedure are tiny and consequently one would obtain quite generally very similar results by using the linearized form in (5.8) as done in [29, 45]. Moreover as stressed in [29] in certain models such a linearized expression could not be sufficiently precise and using (5.10) from the start takes such effects into account.

- For the SM contributions we will use the most recent values for EWPO that include electroweak radiative corrections. Even if the interference terms between SM and NP contributions will not include these corrections, this procedure is justified in view of the smallness of NP effects in 331 models considered by us.

- Comparing SM results with the data we will be able to identify the pattern of deviations from SM predictions and see for which values of β, $\tan\bar{\beta}$ and fermion representations the 331 models can improve the agreement of the theory with the data and what does this imply for our analysis of flavour violating effects.

5.2 Basic formulae for EWPO

The tree level formula for the partial widths is given by

$$\Gamma(Z \to \bar{f}f) = \frac{G_F M_Z^3}{6\pi\sqrt{2}} \left[\frac{\cos^2\theta_W}{g^2}\right] \varrho N_c \left[[\Delta_V^f(Z)]^2_{\text{eff}} + [\Delta_A^f(Z)]^2_{\text{eff}}\right] \tag{5.11}$$

JHEP08(2014)039

with $N_c = 3$ for quarks and $N_c = 1$ for leptons. The additional overall factor relative to formula (2.8) in [29] takes into account the difference in the definitions of the vector and axial-vector couplings summarized above. Defining next $\Gamma_f = \Gamma(Z \to \bar{f}f)$ we have

$$\Gamma_\ell = \Gamma_\mu, \qquad \Gamma_h = 2\Gamma_c + 2\Gamma_u + \Gamma_b, \qquad \Gamma_T = \Gamma_h + 3(\Gamma_\mu + \Gamma_\nu). \tag{5.12}$$

While we do not distinguish between ϱ for b quark contributions and contributions from lighter quarks as such effects are taken into account in the full SM contribution, we separate NP b quark contribution to Γ_h from the one of d and s as transformation properties of the third generation of quarks under $\mathrm{SU}(3)_L$ are different compared to the the first two generations. See the Lagrangian (63) in [3]. This difference has to be taken into account in all observables involving the b quark.

Of interest are then the ratios R_f and the peak cross sections σ_p^f defined as follows

$$R_\ell = \frac{\Gamma_h}{\Gamma_\ell}, \qquad R_b = \frac{\Gamma_b}{\Gamma_h}, \qquad R_c = \frac{\Gamma_c}{\Gamma_h} \qquad \sigma_p^f = \frac{12\pi}{M_Z^2}\frac{\Gamma_e\Gamma_f}{\Gamma_T^2}. \tag{5.13}$$

Note that the definition of R_ℓ differs from the one of R_c and R_b. For the asymmetries A_f we have

$$\mathcal{A}_f = \frac{2[\Delta_A^f(Z)]_{\text{eff}}[\Delta_V^f(Z)]_{\text{eff}}}{[\Delta_V^f(Z)]_{\text{eff}}^2 + [\Delta_A^f(Z)]_{\text{eff}}^2}\,. \tag{5.14}$$

and for the forward-backward asymmetry

$$\mathcal{A}_{\text{FB}}^f = \frac{3}{4}\mathcal{A}_e\mathcal{A}_f\,. \tag{5.15}$$

We would like to warn the reader that similar to [29] our vector and axial-vector couplings for Z and Z' are defined in terms of left-handed and right-handed ones as follows:

$$\Delta_V = \Delta_R + \Delta_L, \qquad \Delta_A = \Delta_R - \Delta_L\,. \tag{5.16}$$

Consequently the axial-vector couplings differ by sign from the ones used in PDG. This implies that also asymmetries $\mathcal{A}_f$ differ by sign from PDG and in table 7 when quoting PDG values we adjusted their definition to our.

From these formulae it is straightforward to derive general analytical formulae for the coefficients $A_\mathcal{O}$ and $B_\mathcal{O}$ in (5.8), valid in any Z' model. We first find in the case of the partial width Γ_f

$$A_{\Gamma_f} = 4\kappa Q^f \frac{v_S^f}{(v_S^f)^2 + (a_S^f)^2} + 1\,, \qquad B_{\Gamma_f} = 2\frac{v_N^f v_S^f + a_N^f a_S^f}{(v_S^f)^2 + (a_S^f)^2}, \tag{5.17}$$

where the second term in A_{Γ_f} is the universal correction from the shift in ϱ in the overall factor in (5.11).

In the case of the asymmetry $\mathcal{A}_f$ the corresponding expressions read

$$A_{\mathcal{A}_f} = 2\kappa\frac{Q^f}{v_S^f}\frac{(a_S^f)^2 - (v_S^f)^2}{(v_S^f)^2 + (a_S^f)^2}\,, \qquad B_{\mathcal{A}_f} = \frac{v_N^f}{v_S^f} + \frac{a_N^f}{a_S^f} - 2\frac{v_N^f v_S^f + a_N^f a_S^f}{(v_S^f)^2 + (a_S^f)^2}\,. \tag{5.18}$$

JHEP08(2014)039

β	$-\frac{2}{\sqrt{3}}$	$-\frac{1}{\sqrt{3}}$	$\frac{1}{\sqrt{3}}$	$\frac{2}{\sqrt{3}}$
$\delta\Gamma_Z$ $[10^{-3}]$	0.132(2.582)	0.0269(1.308)	0.0152(0.578)	0.0949(0.422)
$\delta\sigma_h$ [nbarn $\times 10^{-3}$]	23.48(58.90)	7.678(30.77)	−7.883(16.04)	−24.69(13.00)
δR_ℓ $[10^{-3}]$	−5.250(−7.828)	−2.249(−6.143)	3.395(−5.474)	12.23(−5.339)
$\delta\mathcal{A}_{\rm FB}^{\ell}$ $[10^{-3}]$	0.472(1.838)	0.0924(0.705)	0.0291(0.104)	0.274(−0.0186)
$\delta\mathcal{A}_\ell$ $[10^{-3}]$	−2.084(−7.964)	−0.410(−3.106)	−0.129(−0.463)	−1.215(0.0826)
$\delta\mathcal{A}_c$ $[10^{-3}]$	−0.915(−3.493)	−0.180(−1.364)	−0.0569(−0.203)	−0.533(0.0363)
$\delta\mathcal{A}_b$ $[10^{-3}]$	−0.168(−0.643)	−0.0332(−0.251)	−0.0105(−0.0374)	−0.0983(0.00668)
$\delta\mathcal{A}_{\rm FB}^{c}$ $[10^{-3}]$	1.149(4.408)	0.226(1.714)	0.0713(0.255)	0.670(-0.0455)
$\delta\mathcal{A}_{\rm FB}^{b}$ $[10^{-3}]$	1.482(5.665)	0.292(2.209)	0.0920(0.329)	0.864(−0.0587)
δR_c $[10^{-3}]$	0.0979(0.269)	0.0296(0.132)	−0.0255(0.0584)	−0.0727(0.0432)
δR_b $[10^{-3}]$	0.0950(0.227)	0.0320(0.123)	−0.0348(0.0683)	−0.112(0.0569)
Ω^{331}	17.70(55.25)	15.45(21.32)	16.39(15.20)	19.42(15.02)
Ω^{331}(LEP)	18.29(53.59)	13.95(22.59)	14.42(13.78)	19.08(12.66)
$\delta\sin^2\theta_{\rm eff}^{\ell}$ $[10^{-3}]$	−0.2650(−1.0135)	−0.0522(−0.3950)	−0.0165(−0.0589)	−0.1545(0.01050)

Table 4. Values of the shifts in EWPO for different β and $\tan\bar{\beta} = 1(5)$ in scenario F_1 for fermion representations. We also give the values of Ω^{331} defined in (5.22) and $\delta\sin^2\theta_{\rm eff}^{\ell}$ from (5.29).

Our results in (5.17) and (5.18 agree with the ones one would derive from formulae (6.5)–(6.6) and (7.4)–(7.7) in [44] by dividing them by Γ_f and $\mathcal{A}_f$, respectively.

For R_b and R_c we find respectively

$$A_{R_b} = A_{\Gamma_b} - \left(2\frac{\Gamma_c}{\Gamma_h}A_{\Gamma_c} + 3\frac{\Gamma_b}{\Gamma_h}A_{\Gamma_b}\right), \qquad B_{R_b} = B_{\Gamma_b} - \left(2\frac{\Gamma_c}{\Gamma_h}B_{\Gamma_c} + 3\frac{\Gamma_b}{\Gamma_h}B_{\Gamma_b}\right) \tag{5.19}$$

and

$$A_{R_c} = A_{R_b} + A_{\Gamma_c} - A_{\Gamma_b}, \qquad B_{R_c} = B_{R_b} + B_{\Gamma_c} - B_{\Gamma_b} \tag{5.20}$$

In these formulae Γ_f and Γ_h are just tree-level SM contributions.

We observe that indeed the coefficients $A_{\mathcal{O}}$ depend only on SM couplings and the first term in (5.8) feels the presence of Z' only through $\sin\xi$, while the second one has additional dependence on the diagonal Z' couplings. While these formulae allow an easy comparison with the analyses in [29, 44, 45], in numerical calculations it is easier to use directly (5.10).

5.3 Numerical results

In tables 4–6 we list the shifts in a number of observables as functions of β, $\tan\bar{\beta}$ for the fermion representations F_1 and F_2. In table 7 we summarize SM predictions for these observables, the corresponding data and the pulls as presented after Higgs discovery in [47].

In what follows it will be useful to denote by MI, with a given I=1,... 24, a particular 331 model in which β, $\tan\bar{\beta}$ and fermion representations are fixed. The index I numbers the column in tables 4–6 corresponding to a given model in order of its appearance. Thus we deal with 24 models that we specify in table 8 to make their identification easier. For instance M5 denotes the model with $\beta = 1/\sqrt{3}$, $\tan\bar{\beta} = 1$ and F_1.

JHEP08(2014)039

β	$-\frac{2}{\sqrt{3}}$	$-\frac{1}{\sqrt{3}}$	$\frac{1}{\sqrt{3}}$	$\frac{2}{\sqrt{3}}$
$\delta\Gamma_Z$ $[10^{-3}]$	1.057(4.924)	0.176(1.917)	0.165(0.268)	1.021(−0.0730)
$\delta\sigma_h$ [nbarn $\times 10^{-3}$]	24.18(60.32)	7.795(31.20)	−7.764(15.80)	−23.96(12.62)
δR_ℓ $[10^{-3}]$	−9.294(−17.88)	−2.906(−8.787)	2.737(−4.119)	8.165(−3.168)
$\delta\mathcal{A}_{\rm FB}^{\ell}$ $[10^{-3}]$	0.0375(0.706)	0.0227(0.417)	−0.0405(0.249)	−0.158(0.213)
$\delta\mathcal{A}_\ell$ $[10^{-3}]$	−0.167(−3.108)	−0.101(−1.845)	0.180(−1.104)	0.703(−0.943)
$\delta\mathcal{A}_c$ $[10^{-3}]$	−0.0733(−1.365)	−0.0442(−0.811)	0.0792(−0.485)	0.309(−0.414)
$\delta\mathcal{A}_b$ $[10^{-3}]$	−0.0135(−0.251)	−0.00814(−0.149)	0.0146(−0.0893)	0.0568(−0.0763)
$\delta\mathcal{A}_{\rm FB}^{c}$ $[10^{-3}]$	0.0919(1.715)	0.0554(1.018)	−0.0994(0.609)	−0.387(0.520)
$\delta\mathcal{A}_{\rm FB}^{b}$ $[10^{-3}]$	0.119(2.210)	0.0715(1.312)	−0.128(0.785)	−0.500(0.671)
δR_c $[10^{-3}]$	0.0832(0.232)	0.0273(0.122)	−0.0279(0.0632)	−0.0873(0.0511)
δR_b $[10^{-3}]$	0.105(0.252)	0.0336(0.129)	−0.0332(0.0650)	−0.102(0.0517)
Ω^{331}	14.96(26.29)	15.28(17.77)	16.31(15.90)	18.31(15.76)
Ω^{331}(LEP)	13.04(27.57)	13.26(18.14)	13.77(15.41)	14.74(15.06)
$\delta\sin^2\theta_{\rm eff}^{\ell}$ $[10^{-3}]$	−0.0212(−0.3953)	−0.0128(−0.2347)	0.0229(−0.1404)	0.0893(−0.1200)

Table 5. Values of the shifts in EWPO for different β and $\tan\bar{\beta} = 1(5)$ in scenario F_2 for fermion representations. We also give the values of Ω^{331} defined in (5.22) and $\delta\sin^2\theta_{\rm eff}^{\ell}$ from (5.29).

β	$-\frac{2}{\sqrt{3}}$	$-\frac{1}{\sqrt{3}}$	$\frac{1}{\sqrt{3}}$	$\frac{2}{\sqrt{3}}$
$\delta\Gamma_Z$ $[10^{-3}]$	0.403(−0.092)	0.553(0.244)	1.260(1.869)	2.485(4.831)
$\delta\sigma_h$ [nbarn $\times 10^{-3}$]	−12.76(−13.15)	−16.17(−16.41)	−32.60(−32.14)	−63.39(−61.75)
δR_ℓ $[10^{-3}]$	4.003(6.181)	6.208(7.568)	16.857(14.193)	36.619(26.418)
$\delta\mathcal{A}_{\rm FB}^{\ell}$ $[10^{-3}]$	−0.123(0.108)	−0.027(0.118)	0.445(0.158)	1.322(0.205)
$\delta\mathcal{A}_\ell$ $[10^{-3}]$	0.548(−0.478)	0.119(−0.523)	−1.964(−0.703)	−5.771(−0.908)
$\delta\mathcal{A}_c$ $[10^{-3}]$	0.241(−0.210)	0.052(−0.230)	−0.863(−0.309)	−2.532(−0.399)
$\delta\mathcal{A}_b$ $[10^{-3}]$	0.044(−0.039)	0.010(−0.042)	−0.159(−0.057)	−0.466(−0.073)
$\delta\mathcal{A}_{\rm FB}^{c}$ $[10^{-3}]$	−0.302(0.264)	−0.065(0.288)	1.084(0.387)	3.190(0.500)
$\delta\mathcal{A}_{\rm FB}^{b}$ $[10^{-3}]$	−0.389(0.340)	−0.084(0.372)	1.397(0.500)	4.105(0.645)
δR_c $[10^{-3}]$	−0.048(−0.040)	−0.056(−0.051)	−0.093(−0.102)	−0.163(−0201)
δR_b $[10^{-3}]$	−0.054(−0.059)	−0.070(−0.073)	−0.149(−0.143)	−0.297(−0.272)
Ω^{331}	16.84(17.12)	17.20(17.53)	22.55(20.42)	48.04(29.70)
Ω^{331}(LEP)	13.59(15.72)	14.78(16.20)	23.03(19.37)	48.97(28.94)
$\delta\sin^2\theta_{\rm eff}^{\ell}$ $[10^{-3}]$	0.0697(−0.0608)	0.0151(−0.0665)	−0.2498(−0.0894)	−0.7342(−0.1154)

Table 6. Values of the shifts in EWPO for different β and $\tan\bar{\beta} = 0.2$ in scenario $F_1(F_2)$ for fermion representations. We also give the values of Ω^{331} defined in (5.22) and $\delta\sin^2\theta_{\rm eff}^{\ell}$ from (5.29).

JHEP08(2014)039

Quantity	Input Data	SMfit	Pull
Γ_Z	2.4952(23)	2.4954(14)	0.09
σ_h [nbarn]	41.540(37)	41.479(14)	−1.65
R_ℓ	20.767(25)	20.740(17)	−1.08
$\mathcal{A}_{\rm FB}^{\ell}$	0.0171(10)	0.01627(2)	−0.83
$\mathcal{A}_\ell$(LEP)	−0.1465(33)	−0.1472(7)	−0.2
$\mathcal{A}_\ell$(SLD)	−0.1513(21)	−0.1472(7)	1.95
$\mathcal{A}_\ell$	−0.1499(18)	−0.1472(7)	1.50
$\sin^2\theta_{\rm eff}^{l}$	0.2324(12)	0.23148(10)	−0.7
$\mathcal{A}_c$	−0.670(27)	−0.6679(3)	0.07
$\mathcal{A}_b$	−0.923(20)	−0.93464(5)	−0.58
$\mathcal{A}_{\rm FB}^{c}$	0.0707(35)	0.0738(4)	0.88
$\mathcal{A}_{\rm FB}^{b}$	0.0992(16)	0.1032(5)	2.5
R_c	0.1721(30)	0.17223(6)	0.04
R_b	0.21629(66)	0.21548(5)	−1.23

Table 7. Input Data and SM fit for various EWPO and the pull values. Update of [47].

MI	scen.	β	$\tan\bar{\beta}$	MI	scen.	β	$\tan\bar{\beta}$	MI	scen.	β	$\tan\bar{\beta}$
M1	F_1	$-2/\sqrt{3}$	1	M9	F_2	$-2/\sqrt{3}$	1	M17	F_1	$-2/\sqrt{3}$	0.2
M2	F_1	$-2/\sqrt{3}$	5	M10	F_2	$-2/\sqrt{3}$	5	M18	F_2	$-2/\sqrt{3}$	0.2
M3	F_1	$-1/\sqrt{3}$	1	M11	F_2	$-1/\sqrt{3}$	1	M19	F_1	$-1/\sqrt{3}$	0.2
M4	F_1	$-1/\sqrt{3}$	5	M12	F_2	$-1/\sqrt{3}$	5	M20	F_2	$-1/\sqrt{3}$	0.2
M5	F_1	$1/\sqrt{3}$	1	M13	F_2	$1/\sqrt{3}$	1	M21	F_1	$1/\sqrt{3}$	0.2
M6	F_1	$1/\sqrt{3}$	5	M14	F_2	$1/\sqrt{3}$	5	M22	F_2	$1/\sqrt{3}$	0.2
M7	F_1	$2/\sqrt{3}$	1	M15	F_2	$2/\sqrt{3}$	1	M23	F_1	$2/\sqrt{3}$	0.2
M8	F_1	$2/\sqrt{3}$	5	M16	F_2	$2/\sqrt{3}$	5	M24	F_2	$2/\sqrt{3}$	0.2

Table 8. Definition of the various 331 models.

JHEP08(2014)039

In order to judge the quality of a given model and compare it with the performance of the SM we define for each observable $\mathcal{O}_i$ the *pulls* $P_i^{\rm SM}$ and P_i^{331} as follows

$$P_i^{\rm SM} = \frac{\text{SMfit}_i - (\text{Input Data})_i}{\sigma^i_{\rm exp}}, \qquad P_i^{331} = \frac{\text{SMfit}_i + \delta\mathcal{O}_i - (\text{Input Data})_i}{\sigma^i_{\rm exp}}. \tag{5.21}$$

The pulls $P_i^{\rm SM}$ are the usual ones and their values are given in the last column in table 7. In principle in order to calculate such pulls for every 331 model MI considered by us we would have to repeat the fit of [47] for all models including also other observables that are sensitive to new charged gauge bosons. Such an analysis is clearly beyond the scope of our paper. As $\mathcal{O}_i$ are fixed in a given MI, that is do not introduce new parameters, we expect that such a simplified procedure should give us a correct, even if rough, picture of what is going on.

In order to identify favourite 331 models, as far as electroweak observables are concerned, we define the measures

$$\Omega^{\rm SM} = \sum_i \left(P_i^{\rm SM}\right)^2 = 15.72\ (13.51), \qquad \Omega^{331} = \sum_i \left(P_i^{331}\right)^2 . \tag{5.22}$$

The first SM value is based on table 7 using the average of LEP and SLD values for $\mathcal{A}_\ell$ while the one in the parentheses is obtained by using as curiosity only the LEP value. The values of Ω^{331} for 331 models are given in tables 4–6. The models with smallest Ω^{331} are favoured, while the ones with with largest Ω^{331} disfavoured.

Inspecting these results we make first the following observations when the average of LEP and SLD values for $\mathcal{A}_\ell$ is used.

- All models give small contributions to $\mathcal{A}_c$ and R_c and consequently agree with the data.
- All models give rather small contributions to $\mathcal{A}_b$ and consequently cannot remove the small pull present in the SM. Moreover, M21 and M23 soften the agreement of the theory with data.
- The sizable discrepancy of the SM with the data on R_b cannot be removed in any model. It can be softened by $(0.3 - 0.4)\sigma$ in M2 and M10 and visibly increased in models M21-M24.

We concentrate then our discussion on the remaining observables, where NP effects turn out to be larger. We find

- In most models NP effects in Γ_Z are small in agreement with data. Deviations larger than 1σ are only found in M2, M10 and M23.
- In the case of σ^h the agreement with data is significantly improved in the case of M1, M2, M4, M9, M10, M12 but worsened visibly in M7, M15 and all models with $\tan\bar{\beta} = 0.2$, that is M17-M24.
- Interestingly in the case of R_ℓ all the models with $\tan\bar{\beta} = 0.2$ improve the agreement of the theory with data and this also applies to M7 and M15, while the remaining models slightly worsen the agreement.

JHEP08(2014)039

Pull	M3 $\beta=-\frac{1}{\sqrt{3}}$, F1 $\tan\bar{\beta}=1$	M6 $\beta=\frac{1}{\sqrt{3}}$, F1 $\tan\bar{\beta}=5$	M8 $\beta=\frac{2}{\sqrt{3}}$, F1 $\tan\bar{\beta}=5$	M9 $\beta=-\frac{2}{\sqrt{3}}$, F2 $\tan\bar{\beta}=1$	M11 $\beta=-\frac{1}{\sqrt{3}}$, F2 $\tan\bar{\beta}=1$	M14 $\beta=\frac{1}{\sqrt{3}}$, F2 $\tan\bar{\beta}=5$	M16 $\beta=\frac{2}{\sqrt{3}}$, F2 $\tan\bar{\beta}=5$
P_{Γ_Z}	0.099	0.338	0.271	0.546	0.164	0.204	0.055
P_{σ_h}	−1.441	−1.215	−1.297	−0.995	−1.438	−1.222	−1.308
P_{R_ℓ}	−1.170	−1.299	−1.294	−1.452	−1.196	−1.245	−1.207
$P_{\mathcal{A}^\ell_{\rm FB}}$	−0.737	−0.726	−0.849	−0.792	−0.807	−0.581	−0.617
$P_{\mathcal{A}_\ell}$	1.216	1.187	1.490	1.352	1.389	0.831	0.920
$P_{\mathcal{A}_c}$	0.067	0.067	0.075	0.071	0.072	0.056	0.059
$P_{\mathcal{A}_b}$	−0.584	−0.584	−0.582	−0.583	−0.582	−0.586	−0.586
$P_{\mathcal{A}^c_{\rm FB}}$	0.979	0.987	0.901	0.941	0.930	1.088	1.063
$P_{\mathcal{A}^b_{\rm FB}}$	2.682	2.706	2.463	2.574	2.545	2.991	2.919
P_{R_c}	0.053	0.063	0.058	0.071	0.052	0.064	0.060
P_{R_b}	−1.179	−1.124	−1.141	−1.069	−1.176	−1.129	−1.149

Table 9. Pulls for the seven selected 331 models.

- On the contrary in the case of $\mathcal{A}^\ell_{\rm FB}$ and $\mathcal{A}_\ell$ the models with $\tan\bar{\beta}=1.0$ and $\tan\bar{\beta}=5.0$ are performing much better than the ones with $\tan\bar{\beta}=0.2$. Moreover they perform better than the SM. However, this depends, as discussed below, whether one takes into account the SLD value for $\mathcal{A}_\ell$ or not.

- Concerning $\delta\mathcal{A}^c_{\rm FB}$ and $\delta\mathcal{A}^b_{\rm FB}$ the favourite models listed below introduce only a very small shift to the SM values not improving the status of the theory, while several models, in particular M2, M4, M7, M10, M12, M21 and M23 worsen the agreement with the data. This is also the case of two favoured models below, M14 and M16 but they compensate it through better results for σ^h than obtained within the SM.

The final verdict is given by the values of Ω^{331} in tables 4–6. We observe that seven 331 models have $\Omega^{331}<16.0$. These are in the order of increasing Ω^{331}

$$\text{M9},\quad \text{M8},\quad \text{M6},\quad \text{M11},\quad \text{M3},\quad \text{M16},\quad \text{M14},\qquad \text{(favoured)} \tag{5.23}$$

with the first five performing better than the SM while the last two having basically the same Ω^{331}. The models with *odd* index I correspond to $\tan\bar{\beta}=1.0$ and the ones with *even* one to $\tan\bar{\beta}=5.0$. We list the pulls P_i^{331} in these seven models in table 9.

As seen in this table all favoured models improve the agreement of the theory with data on σ^h. This is in particular the case of M9 and this fact is primarily responsible why M9 wins the competition as it does reasonably well for other observables. We also observe that all favoured models, except M8, improve the agreement of theory with data on $\mathcal{A}^\ell_{\rm FB}$ and $\mathcal{A}_\ell$. However the models M14 and M16 which perform best in this respect are not the top models as they perform worse than the first ones on other observables which basically

JHEP08(2014)039

do not provide any improvements on these asymmetries. The reason is that M14 and M16 experience difficulties with $\delta\mathcal{A}^c_{\rm FB}$ and $\delta\mathcal{A}^b_{\rm FB}$, as stated above, making the agreement of the theory with data to be worse than in the SM.

Yet, as discussed below, our analysis confirms the general findings of Richard [43] that in 331 models the departure of the data on $\mathcal{A}^\ell_{\rm FB}$ and $\mathcal{A}_\ell$ from their SM values is correlated within 331 models with the $B_d \to K^*\mu^+\mu^-$ anomaly, even if the model M2 which he studied is basically excluded by other electroweak data when correct expression for $\sin\xi$ is used. This is in particular the case of Γ_Z and $\mathcal{A}^b_{\rm FB}$. Otherwise this model is interesting as it removes the discrepancy of the SM with the data on σ^h.

An important result of our analysis is the weak performance of models with $\tan\bar\beta = 0.2$, although the models M17-M20 cannot be excluded. The models which definitely have difficulties with electroweak precision data are

$$\text{M2,}\quad \text{M4,}\quad \text{M7,}\quad \text{M10,}\quad \text{M21,}\quad \text{M22,}\quad \text{M23,}\quad \text{M24,}\qquad \text{(disfavoured)} \tag{5.24}$$

Looking at these results we conclude that from the point of view of electroweak precision tests the following combinations of the values of β, $\tan\bar\beta$ and fermion representations are favoured.

- Three models with $\beta = -2/\sqrt{3}$ and $\beta = -1/\sqrt{3}$ for $\tan\beta = 1.0$. For F_1 this is M3 with $\beta = -1/\sqrt{3}$ and for F_2 M9 and M11 for $\beta = -2/\sqrt{3}$ and $\beta = -1/\sqrt{3}$, respectively.

- Four models with $\beta = 1/\sqrt{3}$ and $\beta = 2/\sqrt{3}$ for $\tan\beta = 5.0$. For F_1 these are M6 and M8 for $\beta = 1/\sqrt{3}$ and $\beta = 2/\sqrt{3}$, respectively and analogously M14 and M16 in the case for F_2.

It should be emphasized that all these seven models pass the present electroweak tests for $M_{Z'} = 3\,\text{TeV}$ as well as the SM or in five cases even better than it. Even if the models with $\beta = \pm 2/\sqrt{3}$ perform slightly better than the ones with $\beta = \pm 1/\sqrt{3}$ it is not possible on the basis of Ω^{331} alone to identify the winner among them. On the other hand one day this should be possible on the basis of the table 9 once various questions related to measurements at LEP and SLD will be clarified. As demonstrated below flavour physics can offer definite help in this context.

In the latter context it is interesting to observe that if the LEP result for $\mathcal{A}_\ell$ would be the true one five models on the list of favourites in (5.23) would remain

$$\text{M8,}\quad \text{M9,}\quad \text{M11,}\quad \text{M17,}\quad \text{M13,}\quad \text{M6,}\quad \text{M3,}\qquad \text{(LEP favoured)} \tag{5.25}$$

with the first three performing better than the SM. M14 and M16 are not present anymore on this list because they favoured SLD result. Instead M13 and in particular M17 with $\tan\bar\beta = 0.2$ are among favourites. As we will discuss below M17 has a unique property among the favourites as far as flavour physics is concerned.

JHEP08(2014)039

5.4 The issue of $\sin^2\theta^\ell_{\rm eff}$

In testing the SM one can define $\sin^2\theta^\ell_{\rm eff}$ by using SM tree-level expression for $\mathcal{A}_\ell$. This parameter is most precisely extracted from the data on $\mathcal{A}_\ell$ and $\mathcal{A}^b_{\rm FB}$ but also from $\mathcal{A}^\ell_{\rm FB}$. Unfortunately the determinations of $\sin^2\theta^\ell_{\rm eff}$ from these observables are really not in agreement with each other. On one hand in the case of $\mathcal{A}_\ell$ we have [43, 48]

$$\sin^2\theta^\ell_{\rm eff}({\rm SLD}) = 0.23098(26), \qquad \sin^2\theta^\ell_{\rm eff}({\rm LEP}) = 0.23159(41) \tag{5.26}$$

and from forward-backward asymmetries $\mathcal{A}^\ell_{\rm FB}$ and $\mathcal{A}^b_{\rm FB}$ one finds respectively

$$\sin^2\theta^\ell_{\rm eff} = 0.23099(53), \qquad \sin^2\theta^\ell_{\rm eff} = 0.23221(29). \tag{5.27}$$

This implies roughly 3σ discrepancy between the two most precise determinations. The resulting values from all data as given in table 7 are

$$\sin^2\theta^\ell_{\rm eff}({\rm EXP}) = 0.2324(12), \qquad \sin^2\theta^\ell_{\rm eff}({\rm SM}) = 0.23148(10). \tag{5.28}$$

Consequently there is some preference for the positive shift in $\sin^2\theta^\ell_{\rm eff}$ relative to the best SM value.

Until now we did not look at $\sin^2\theta^\ell_{\rm eff}$ in 331 models and calculated $\mathcal{A}^\ell_{\rm FB}$, $\mathcal{A}_\ell$, $\mathcal{A}^b_{\rm FB}$ and other observables directly to judge the quality of a given model on the basis of them. But it is instructive to calculate the shift of $\sin^2\theta^\ell_{\rm eff}$ due to NP contributions for 24 models considered by us using the operative definition [48]

$$\delta\sin^2\theta^\ell_{\rm eff} = \frac{1}{4}\left(1+\frac{[\Delta^\ell_V(Z)]_{\rm eff}}{[\Delta^\ell_A(Z)]_{\rm eff}}\right) - \sin^2\theta_W, \tag{5.29}$$

where in the effective vector couplings the shift (5.9) has to be included. An extensive discussion of $\sin^2\theta^\ell_{\rm eff}$ can be found in [48] where further references can be found. See also [43]. In writing (5.29) we have adjusted the sign in the formula (8.3) in [48] to our definition of the axial-vector coupling.

The shift in $\delta\sin^2\theta^\ell_{\rm eff}$ in 331 models comes first from the shift of $\sin^2\theta_W$ which as seen in (5.7) is negative in 331 models and in any Z' model. But in addition to this shift, which comes from $\Delta\varrho_M$ and affects only vector couplings, both vector and axial-vector couplings receive modifications from the mixing with Z', that is the shifts in the couplings proportional to $\sin\xi$ and involving Z' couplings.

The result of this exercise is given in the last rows in tables 4–6. The striking feature is that out of 24 models 19 give a negative shift of $\sin^2\theta^\ell_{\rm eff}$, while only 5 a positive one. These are M8, M13, M15, M17 and M19.

It is not surprising that M8, M13 and M17 perform here so well as they are on the list of LEP favourites in (5.25). What is remarkable that M8 is the only among our favourite models in (5.23) that gives a positive shift of $\sin^2\theta^\ell_{\rm eff}$. But this shift being 1×10^{-5} is totally negligible. Yet, this model similar to all models with positive shift is fully compatible with the experimental value in (5.28).

JHEP08(2014)039

We also note that models M14 and M16 on our list of favourites give

$$\sin^2\theta_{\rm eff}^{\ell}(\mathrm{M14}) = 0.23134, \qquad \sin^2\theta_{\rm eff}^{\ell}(\mathrm{M16}) = 0.23136, \tag{5.30}$$

where we have added the corresponding shifts to the SM value in (5.28). These values are within 1.5σ from the central value of $\sin^2\theta_{\rm eff}^{\ell}$ from the SLD.

We also confirm qualitatively the finding in [43] that the model M2 provides a shift that results in $\sin^2\theta_{\rm eff}^{\ell}$ close to the SLD result. We find 0.23122 and 0.23048 for $\tan\bar{\beta} = 1.0$ and $\tan\bar{\beta} = 5.0$, respectively. For $\tan\bar{\beta} \approx 3.0$ the SLD result can be well reproduced. However, this model has problems with other observables as we have seen above.

While we do not think that just looking at $\sin^2\theta_{\rm eff}^{\ell}$ offers a fully transparent test of a given extension of the SM, the rather different values of this parameter extracted from different observables calls for future improved measurements of EWPO which hopefully one day will be possible at a future ILC. This, as stressed in [43], could offer powerful tests of 331 models.

5.5 Implications for flavour physics

Our analysis of EWPO identified a group of seven models among 24 considered by us and the question arises whether flavour physics could distinguish between them. As we will now discuss our analysis in previous sections demonstrates this rather clearly and having the plots presented there we can summarize how the seven models in question could be distinguished by flavour observables in the coming flavour precision era.

Let us first summarize the main message from our analysis of EWPO which is related to the fact that the values $\tan\bar{\beta} = 0.2$ are disfavoured:

- Significant NP effects in B and K decays to neutrinos seem rather unlikely, even if the branching ratio for $K_L \to \pi^0\nu\bar{\nu}$ could still be modified by 15%. In turn due to the correlation with ε'/ε also NP effects in this ratio are predicted to be small implying that $B_6^{(1/2)} \approx 1.0$ in order to agree with data. On the other hand as discussed in our recent paper [38] the required precise value of this parameter depends on the values of $|V_{cb}|$ and $|V_{ub}|$.

- The most interesting NP effects are found in $B \to K^*\mu^+\mu^-$ and $B_{s,d} \to \mu^+\mu^-$ and we will confine the discussion of the favourite models in (5.23) to these decays.

The selection of favourite models and the comments just made imply that it is sufficient to look at figures 2 and 3 for F_1 and F_2, respectively. The results for the seven favourite models can be found there with only the results in the upper left panel in figure 2 being disfavoured. In the remaining seven panels in these two figures, the results for our favourite models are simply identified by selecting the $\tan\bar{\beta} = 1.0$ line (lighter colours) in the case of $\beta < 0$ and the $\tan\bar{\beta} = 5.0$ line (darker colours) in the case of $\beta > 0$. The main implications for rare B decays are then as follows:

- A significant suppression of $\mathcal{B}(B_s \to \mu^+\mu^-)$ and significant negative shift in $\mathrm{Re}C_9^{\rm NP}$ cannot take place simultaneously. This would be possible in M2 but this model belongs to disfavoured ones by our EWPO analysis.

JHEP08(2014)039

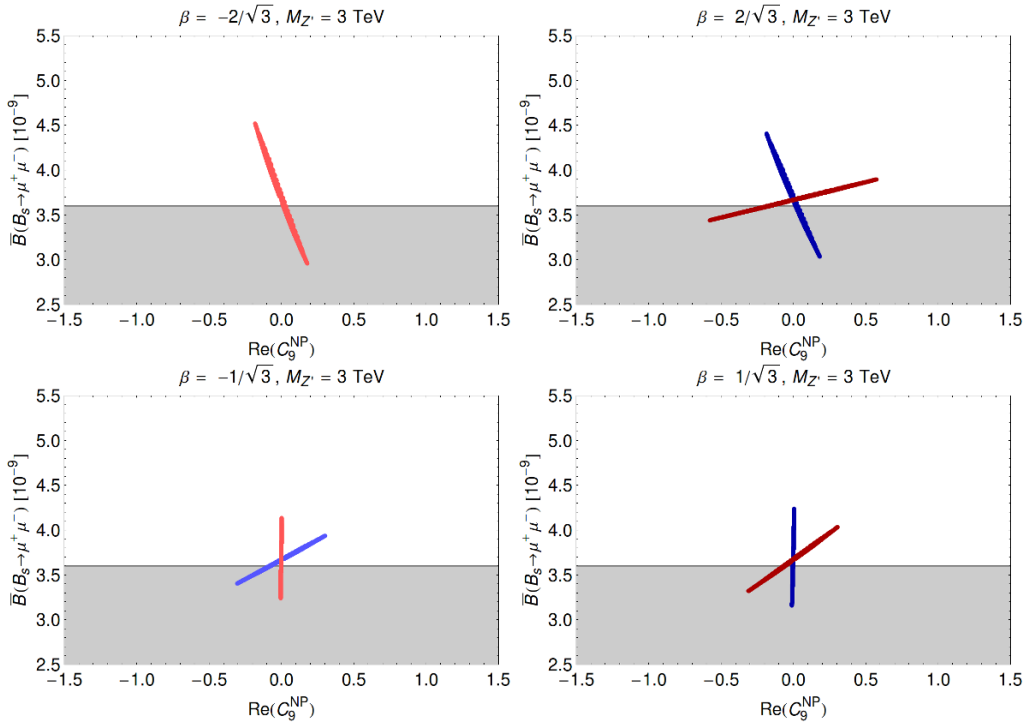

Figure 15. $\overline{\mathcal{B}}(B_s \to \mu^+\mu^-)$ versus $\mathrm{Re}(\mathrm{C}_9^{\mathrm{NP}})$ for the favourite models from table 9 for F1 (blue) and F2 (red) and $\tan\bar{\beta} = 1(5)$ with lighter (darker) colours.

- For softening the $B_d \to K^*\mu^+\mu^-$ anomaly the most interesting is the model M16, that is the model with F_2, $\beta = 2/\sqrt{3}$ and $\tan\bar{\beta} = 5.0$. See upper right panel in figure 3. The usual statements present in the literature [4, 26, 43] that the 331 models with negative β are most powerful in this case apply to F_1 representations. But as our analysis shows the model M2 with $\beta = -2/\sqrt{3}$ considered by us in [4] is disfavoured by the EWPO analysis.

- If the anomaly in question remains but decreases with time also model M3 (left lower panel in figure 2) and M14 (right lower panel in figure 3) would be of interest.

- The remaining four models, in fact the four top models on our list of favourites in (5.23), do not provide any explanation of $B_d \to K^*\mu^+\mu^-$ anomaly but are interesting for $B_{s,d} \to \mu^+\mu^-$ decays. These are M6, M8, M9 and M11, the first two with F_1 and the last two with F_2 fermion representation. The differences between these models as far as $B_s \to \mu^+\mu^-$ is concerned are most transparently seen in figures 4 and 5 from which we conclude that the strongest suppression of the rate for $B_s \to \mu^+\mu^-$ can be achieved in M8 and M9. M8 result is shown in the right upper panels in figures 2 and 4 and M9 result in the left upper panels of in figures 3 and 5. In fact these two models are the two leaders on the list of favourites in (5.23). The suppression of the $B_s \to \mu^+\mu^-$ rate is smaller in M6 and M11 as seen in lower right and lower left panels in figures 2 and 3, respectively.

JHEP08(2014)039

We observe that flavour physics can clearly distinguish between the favourite models selected by EWPO analysis. We summarize it in figure 15, where only the results in the seven favourite models are shown. If the $B_d \to K^*\mu^+\mu^-$ anomaly will persist the winner will be M16 which is represented in this figure by the dark red line in the upper right panel. If it disappears but suppression of the rate for $B_s \to \mu^+\mu^-$ will be required the winners will be M8 and M9, the blue and red lines in the upper right and upper left panel in figure 15, respectively. It is interesting that the combination of future flavour data and EWPO tests can rather clearly indentify one or two favourite 331 models among 24 cases considered by us.

An interesting situation would also arise if the LEP result for $\mathcal{A}_\ell$ would turn out to be the correct one. In this case M14 and M16 are no longer among favourites as seen in (5.25) and are replaced by M13 and M17. M13 is a good replacement for M14 as it also allows moderate softening of the $B_d \to K^*\mu^+\mu^-$ anomaly as seen in the right lower panel in figure 3. But more interesting is M17. Indeed as seen in the upper left panel in figure 2 for $\tan\bar{\beta} = 0.2$ (gray line) the $B_d \to K^*\mu^+\mu^-$ anomaly can be softened as much as it was possible in the case of M16. But as seen in the upper left panel in figure 10 (purple line) in this model with F_1 representations also significant NP effects in $K_L \to \pi^0\nu\bar{\nu}$ are possible. Smaller NP effects, as seen in figure 12, are found in the case of F_2 but $M18$ is not among the favourite models anyway. All this again shows an important interplay between flavour observables and electroweak precision tests.

6 Summary and conclusions

In this paper we have addressed the question whether in 331 models the FCNCs due to Z tree-level exchanges generated through $Z - Z'$ mixing could play any significant role in flavour physics. Actually it is known from the flavour analyses of Randall-Sundrum models with custodial protection (RSc) [49, 50], that while $\Delta F = 2$ processes are governed by heavy Kaluza-Klein gauge bosons with and without colour, NP contributions in $\Delta F = 1$ processes are governed by induced right-handed flavour-violating Z couplings.

Here we analyzed several 331 models which have a much smaller number of parameters than RSc and this allows to see more transparently various NP effects than in the latter scenario. As our basic formula for the $Z - Z'$ in 331 model differs from the one found in the literature [8, 14, 43] we have reconsidered some aspects of constraints from EWPO. Moreover we have identified for the first time various correlations between flavour and electroweak physics that depend on the parameters of 331 model, in particular, β, $\tan\bar{\beta}$, $M_{Z'}$ and the fermion representations.

As far as flavour physics is concerned our main findings are as follows:

- NP contributions to $\Delta F = 2$ transitions and decays like $B \to K^*\ell^+\ell^-$ are governed by Z' tree-level exchanges. Therefore for these processes our analysis in [4] remains unchanged. But as we summarize below our analysis of EWPO casts some shadow on some of these models.

- On the other hand for $B_{s,d} \to \mu^+\mu^-$ decays Z contributions can be important. We find that for $\tan\bar{\beta} = 5.0$ these contributions interfere constructively with Z' contri-

JHEP08(2014)039

butions enhancing NP effects, while for low $\tan\bar{\beta} = 0.2$ Z contributions practically cancel the ones from Z'. Similar dependence on $\tan\bar{\beta}$ is found for $K_L \to \mu^+\mu^-$.

- Similarly Z boson tree-level contributions to $B_{s,d}$ and K decays with neutrinos in the final state can be relevant but in this case the $\tan\bar{\beta}$ dependence is opposite to the one found for $B_{s,d} \to \mu^+\mu^-$. We find that for $\tan\bar{\beta} = 5.0$ these contributions practically cancel the ones from Z' but for low $\tan\bar{\beta} = 0.2$ Z contributions interfere constructively with Z' contributions enhancing NP effects. In particular as seen in figures 10 and 11 in the case of $K_L \to \pi^0\nu\bar{\nu}$ NP effects can amount to 30% at the level of the branching ratio when the constraints from EWPO are not taken into account.

- As a result of this opposite dependence on $\tan\bar{\beta}$ the correlations between decays with muons and neutrinos in the final state exhibit significant dependence on $\tan\bar{\beta}$ and can serve to determine this parameter in the future. See in particular figures 4 and 5.

- Our analysis of ε'/ε is to our knowledge the first one in 331 models. Including both Z' and Z contributions we find that the former dominate. But NP effects are not large and in order to fit the data $B_6^{(1/2)} \approx 1.0$ is favoured.

- We also find a strict correlation between ε'/ε and $\mathcal{B}(K_L \to \pi^0\nu\bar{\nu})$. The interesting feature here, as seen in figure 14, is the decrease of ε'/ε with increasing $\mathcal{B}(K_L \to \pi^0\nu\bar{\nu})$ for *negative* β and its increase with increasing $\mathcal{B}(K_L \to \pi^0\nu\bar{\nu})$ for *positive* β.

- Performing the analysis for different fermion representations we find that for certain observables this dependence is significant. As an example the comparison of the plots in figures 2 and 3 demonstrates the breakdown of the invariance under (2.16) by $Z - Z'$ mixing.

As far as electroweak physics is concerned our main findings are as follows:

- Seven among 24 combinations of β, $\tan\bar{\beta}$ and fermion representation F_1 or F_2 provide better or equally good description of the electroweak precision data compared with the SM. However, none of these models allows for the explanation of the 2.5σ departures of $\mathcal{A}_{\rm FB}^b$ and R_b from the SM but several of them improve significantly the agreement of the theory with the average of SLD and LEP data for A_l.

- Among these models none of them allows to simultaneously suppress the rate for $B_s \to \mu^+\mu^-$ and soften the $B_d \to K^*\mu^+\mu^-$ anomaly.

- On the other hand there are few models which either suppress the rate for $B_s \to \mu^+\mu^-$ or soften the $B_d \to K^*\mu^+\mu^-$ anomaly.

- None of these models allows significant NP effects in B and K decays with neutrinos in the final state although departures by 15% relative to the SM prediction for the rate of $K_L \to \pi^0\nu\bar{\nu}$ are still possible.

JHEP08(2014)039

- Assuming that the LEP result for $\mathcal{A}_\ell$ is the correct one, we have found that in this case NP effects in $K_L \to \pi^0 \nu\bar{\nu}$ are larger than when both LEP and SLD results are taken into account.

Our analysis shows that the interplay of flavour physics and EWPO tests can significantly constrain NP models, in particular those with not too many free parameters. We are looking forward to coming years in order to see whether the 331 models will survive improved flavour data and in particular whether Z' will be discovered at the LHC. The correlations presented by us should allow to monitor transparently future developments in the data.

Acknowledgments

We would like to thank Christoph Niehoff and David Straub for asking us about the size of tree-level Z contributions to FCNC processes in 331 models. We also thank Guido Altarelli, Jernej Kamenik, Ulrich Nierste, Francois Richard, R. Martinez and F. Ochoa for interesting discussions. This research was done and financed in the context of the ERC Advanced Grant project "FLAVOUR"(267104) and was partially supported by the DFG cluster of excellence "Origin and Structure of the Universe".

References

[1] F. Pisano and V. Pleitez, *An* SU(3) × U(1) *model for electroweak interactions*, *Phys. Rev.* **D 46** (1992) 410 [hep-ph/9206242] [INSPIRE].

[2] P.H. Frampton, *Chiral dilepton model and the flavor question*, *Phys. Rev. Lett.* **69** (1992) 2889 [INSPIRE].

[3] A.J. Buras, F. De Fazio, J. Girrbach and M.V. Carlucci, *The anatomy of quark flavour observables in* 331 *models in the flavour precision era*, *JHEP* **02** (2013) 023 [arXiv:1211.1237] [INSPIRE].

[4] A.J. Buras, F. De Fazio and J. Girrbach, 331 *models facing new* $b \to s\mu^+\mu^-$ *data*, *JHEP* **02** (2014) 112 [arXiv:1311.6729] [INSPIRE].

[5] D. Ng, *The electroweak theory of* SU(3) × U(1), *Phys. Rev.* **D 49** (1994) 4805 [hep-ph/9212284] [INSPIRE].

[6] R.A. Diaz, R. Martinez and F. Ochoa, *The scalar sector of the* $\mathrm{SU}(3)_c \times \mathrm{SU}(3)_L \times \mathrm{U}(1)_X$ *model*, *Phys. Rev.* **D 69** (2004) 095009 [hep-ph/0309280] [INSPIRE].

[7] J.T. Liu and D. Ng, *Lepton flavor changing processes and CP-violation in the* 331 *model*, *Phys. Rev.* **D 50** (1994) 548 [hep-ph/9401228] [INSPIRE].

[8] R.A. Diaz, R. Martinez and F. Ochoa, $\mathrm{SU}(3)_c \times \mathrm{SU}(3)_L \times \mathrm{U}(1)_X$ *models for beta arbitrary and families with mirror fermions*, *Phys. Rev.* **D 72** (2005) 035018 [hep-ph/0411263] [INSPIRE].

JHEP08(2014)039

[9] F. Ochoa and R. Martinez, *$Z - Z'$ mixing in $\mathrm{SU}(3)_c \times \mathrm{SU}(3)_L \times \mathrm{U}(1)_X$ models with beta arbitrary*, hep-ph/0508082 [INSPIRE].

[10] J.T. Liu, *Generation nonuniversality and flavor changing neutral currents in the 331 model*, *Phys. Rev.* **D 50** (1994) 542 [hep-ph/9312312] [INSPIRE].

[11] J.A. Rodriguez and M. Sher, *FCNC and rare B decays in 331 models*, *Phys. Rev.* **D 70** (2004) 117702 [hep-ph/0407248] [INSPIRE].

[12] C. Promberger, S. Schatt and F. Schwab, *Flavor changing neutral current effects and CP-violation in the minimal 331 model*, *Phys. Rev.* **D 75** (2007) 115007 [hep-ph/0702169] [INSPIRE].

[13] J. Agrawal, P.H. Frampton and J.T. Liu, *The decay $b \to s\gamma$ in the 331 model*, *Int. J. Mod. Phys.* **A 11** (1996) 2263 [hep-ph/9502353] [INSPIRE].

[14] A.E. Carcamo Hernandez, R. Martinez and F. Ochoa, *Z and Z' decays with and without FCNC in 331 models*, *Phys. Rev.* **D 73** (2006) 035007 [hep-ph/0510421] [INSPIRE].

[15] C. Promberger, S. Schatt, F. Schwab and S. Uhlig, *Bounding the minimal 331 model through the decay $B \to X_s\gamma$*, *Phys. Rev.* **D 77** (2008) 115022 [arXiv:0802.0949] [INSPIRE].

[16] M. Singer, J.W.F. Valle and J. Schechter, *Canonical neutral current predictions from the weak electromagnetic gauge group $\mathrm{SU}(3) \times \mathrm{U}(1)$*, *Phys. Rev.* **D 22** (1980) 738 [INSPIRE].

[17] J.W.F. Valle and M. Singer, *Lepton number violation with quasi Dirac neutrinos*, *Phys. Rev.* **D 28** (1983) 540 [INSPIRE].

[18] S.M. Boucenna, S. Morisi and J.W.F. Valle, *Radiative neutrino mass in 331 scheme*, *Phys. Rev.* **D 90** (2014) 013005 [arXiv:1405.2332] [INSPIRE].

[19] A.J. Buras, F. De Fazio and J. Girrbach, *The anatomy of Z' and Z with flavour changing neutral currents in the flavour precision era*, *JHEP* **02** (2013) 116 [arXiv:1211.1896] [INSPIRE].

[20] A.J. Buras and J. Girrbach, *Left-handed Z' and Z FCNC quark couplings facing new $b \to s\mu^+\mu^-$ data*, *JHEP* **12** (2013) 009 [arXiv:1309.2466] [INSPIRE].

[21] LHCb collaboration, *Differential branching fraction and angular analysis of the decay $B^0 \to K^{*0}\mu^+\mu^-$*, *JHEP* **08** (2013) 131 [arXiv:1304.6325] [INSPIRE].

[22] LHCb collaboration, *Measurement of form-factor-independent observables in the decay $B^0 \to K^{*0}\mu^+\mu^-$*, *Phys. Rev. Lett.* **111** (2013) 191801 [arXiv:1308.1707] [INSPIRE].

[23] LHCb collaboration, *Measurement of the $B_s^0 \to \mu^+\mu^-$ branching fraction and search for $B^0 \to \mu^+\mu^-$ decays at the LHCb experiment*, *Phys. Rev. Lett.* **111** (2013) 101805 [arXiv:1307.5024] [INSPIRE].

[24] CMS collaboration, *Measurement of the $B_s \to \mu^+\mu^-$ branching fraction and search for $B_0 \to \mu^+\mu^-$ with the CMS experiment*, *Phys. Rev. Lett.* **111** (2013) 101804 [arXiv:1307.5025] [INSPIRE].

[25] CMS and LHCb collaborations, *Combination of results on the rare decays $B^0_{(s)} \to \mu^+\mu^-$ from the CMS and LHCb experiments*, CMS-PAS-BPH-13-007, CERN, Geneva Switzerland (2013).

[26] R. Gauld, F. Goertz and U. Haisch, *An explicit Z'-boson explanation of the $B \to K^*\mu^+\mu^-$ anomaly*, *JHEP* **01** (2014) 069 [arXiv:1310.1082] [INSPIRE].

JHEP08(2014)039

[27] P. Langacker, *The physics of heavy Z' gauge bosons*, *Rev. Mod. Phys.* **81** (2009) 1199 [arXiv:0801.1345] [INSPIRE].

[28] J. Erler, P. Langacker, S. Munir and E. Rojas, *Improved constraints on Z' bosons from electroweak precision data*, *JHEP* **08** (2009) 017 [arXiv:0906.2435] [INSPIRE].

[29] G. Altarelli, N. Di Bartolomeo, F. Feruglio, R. Gatto and M.L. Mangano, *R_b, R_c and jet distributions at the Tevatron in a model with an extra vector boson*, *Phys. Lett.* **B 375** (1996) 292 [hep-ph/9601324] [INSPIRE].

[30] R. Martinez and F. Ochoa, *Constraints on* 331 *models with electroweak Z pole observables and Z' search at LHC*, arXiv:1405.4566 [INSPIRE].

[31] C. Bobeth et al., *$B_{s,d} \to \ell^+\ell^-$ in the Standard Model with reduced theoretical uncertainty*, *Phys. Rev. Lett.* **112** (2014) 101801 [arXiv:1311.0903] [INSPIRE].

[32] S. Descotes-Genon, J. Matias and J. Virto, *Understanding the $B \to K^*\mu^+\mu^-$ anomaly*, *Phys. Rev.* **D 88** (2013) 074002 [arXiv:1307.5683] [INSPIRE].

[33] W. Altmannshofer and D.M. Straub, *New physics in $B \to K^*\mu\mu$?*, *Eur. Phys. J.* **C 73** (2013) 2646 [arXiv:1308.1501] [INSPIRE].

[34] F. Beaujean, C. Bobeth and D. van Dyk, *Comprehensive Bayesian analysis of rare (semi)leptonic and radiative B decays*, *Eur. Phys. J.* **C 74** (2014) 2897 [arXiv:1310.2478] [INSPIRE].

[35] HPQCD collaboration, C. Bouchard, G.P. Lepage, C. Monahan, H. Na and J. Shigemitsu, *Standard Model predictions for $B \to K\ell^+\ell^-$ with form factors from lattice QCD*, *Phys. Rev. Lett.* **111** (2013) 162002 [arXiv:1306.0434] [INSPIRE].

[36] HPQCD collaboration, C. Bouchard, G.P. Lepage, C. Monahan, H. Na and J. Shigemitsu, *Rare decay $B \to K\ell^+\ell^-$ form factors from lattice QCD*, *Phys. Rev.* **D 88** (2013) 054509 [arXiv:1306.2384] [INSPIRE].

[37] M. Patel, *Latest rare decays results from LHCb*, talk given at *Moriond-Electroweak*, LHCb-TALK-2014-043, La Thuile Italy March 16 2014.

[38] A.J. Buras, F. De Fazio and J. Girrbach, *$\Delta I = 1/2$ rule, ε'/ε and $K \to \pi\nu\bar{\nu}$ in $Z'(Z)$ and G' models with FCNC quark couplings*, arXiv:1404.3824 [INSPIRE].

[39] A.J. Buras and M. Jamin, *ε'/ε at the NLO:* 10 *years later*, *JHEP* **01** (2004) 048 [hep-ph/0306217] [INSPIRE].

[40] T. Blum et al., *Lattice determination of the $K \to (\pi\pi)_{I=2}$ decay amplitude A_2*, *Phys. Rev.* **D 86** (2012) 074513 [arXiv:1206.5142] [INSPIRE].

[41] S. Aoki et al., *Review of lattice results concerning low energy particle physics*, arXiv:1310.8555 [INSPIRE].

[42] V. Cirigliano, A. Pich, G. Ecker and H. Neufeld, *Isospin violation in ε'*, *Phys. Rev. Lett.* **91** (2003) 162001 [hep-ph/0307030] [INSPIRE].

[43] F. Richard, *A Z' interpretation of $B_d \to K^*\mu^+\mu^-$ data and consequences for high energy colliders*, arXiv:1312.2467 [INSPIRE].

[44] G. Altarelli, R. Casalbuoni, D. Dominici, F. Feruglio and R. Gatto, *Testing for heavier vector bosons in e^+e^- at Z peak: a comparative study of different models*, *Nucl. Phys.* **B 342** (1990) 15 [INSPIRE].

JHEP08(2014)039

[45] P. Chiappetta, J. Layssac, F.M. Renard and C. Verzegnassi, *Hadrophilic Z': a bridge from LEP-1, SLC and CDF to LEP-2 anomalies*, *Phys. Rev.* **D 54** (1996) 789 [hep-ph/9601306] [INSPIRE].

[46] H.N. Long and T. Inami, *S, T, U parameters in $\mathrm{SU}(3)_C \times \mathrm{SU}(3)_L \times \mathrm{U}(1)$ model with right-handed neutrinos*, *Phys. Rev.* **D 61** (2000) 075002 [hep-ph/9902475] [INSPIRE].

[47] M. Baak et al., *The electroweak fit of the Standard Model after the discovery of a new boson at the LHC*, *Eur. Phys. J.* **C 72** (2012) 2205 [arXiv:1209.2716] [INSPIRE].

[48] R. Tenchini and C. Verzegnassi, *The physics of the Z and W bosons*, World Scientific, Singapore (2007).

[49] M. Blanke, A.J. Buras, B. Duling, K. Gemmler and S. Gori, *Rare K and B decays in a warped extra dimension with custodial protection*, *JHEP* **03** (2009) 108 [arXiv:0812.3803] [INSPIRE].

[50] M. Bauer, S. Casagrande, U. Haisch and M. Neubert, *Flavor physics in the Randall-Sundrum model: II. Tree-level weak-interaction processes*, *JHEP* **09** (2010) 017 [arXiv:0912.1625] [INSPIRE].

JHEP08(2014)039